THE JOURNAL OF PHYSICAL CHEMISTRY B
A JOURNAL OF THE AMERICAN CHEMICAL SOCIETY

pubs.acs.org/JPCB

Article

Real-Time Confocal Imaging of Rare Morphological Transitions in Protein-free GUVs Uncovers Shallow Energy Landscapes for Membrane Assemblies

Published as part of The Journal of Physical Chemistry B special issue "At the Cutting Edge of Theoretical and Computational Biophysics".

Akanksha Chauhan* and Aditya Mittal*

Cite This: *J. Phys. Chem. B* 2025, 129, 12702−12714

Read Online

ACCESS | Metrics & More | Article Recommendations | Supporting Information

ABSTRACT: Lipid vesicles exhibit a rich variety of morphologies shaped by the interplay of composition, curvature, and mechanical perturbations. In this study, we study rare spontaneous morphological remodeling events in phase separating (POPC:DPPC) and non-phase separating (POPC:DOPE) protein-free giant unilamellar vesicles (GUVs), under apparently unperturbed (isothermal/physical and chemical) conditions using real-time confocal microscopy. Quantitative analysis of these events through geometric analysis and Canham−Helfrich elastic energy modeling revealed two distinct mechanistic classes of morphological transformations: those with stable elastic energy profiles (occurring over shallow energy landscapes) and, energetically dissipative relaxations (after possible transient mechanical perturbations from sample handling). The study highlights how lipid composition alone can endow membranes with dynamic shape plasticity, underscoring the role of curvature-composition coupling in accessing metastable morphologies, thereby allowing kinetic windows for stabilization of specific morphologies with compositional interventions. These findings offer new insight into how membranes may respond to subtle environmental cues and how early prebiotic membranes or protein-free compartments might have sampled and stabilized complex shapes in cellular evolution.

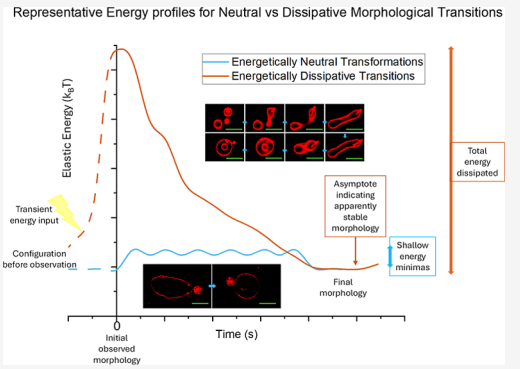

Downloaded via INDIAN INST OF TECH DELHI- IIT on February 18, 2026 at 13:39:57 (UTC).
See https://pubs.acs.org/sharingguidelines for options on how to legitimately share published articles.

INTRODUCTION

The dynamic remodeling of cellular membranes is fundamental to life processes such as endocytosis, exocytosis, organelle biogenesis, vesicle trafficking, and cell division. These shape changes are not only critical for maintaining compartmentalization and material transport within living cells but are also central to understanding how primitive cells may have emerged and evolved. Early protocells have been hypothesized to be devoid of a protein-based machinery, enveloped primarily by lipid membranes, and possibly relied on intrinsic membrane properties and environmental fluctuations to drive morphological transitions.[1,2] Studying spontaneous remodeling events in lipid membranes thus provides valuable insight into both the biophysical mechanisms that govern cellular behavior and the prebiotic conditions that may have enabled primitive compartment dynamics.

The biophysical origins of membrane shape transformations have intrigued researchers since Canham's seminal work in the 1970s, which proposed that the distinctive biconcave shape of red blood cells results from the minimization of membrane bending energy.[3,4] This diverse spectrum of morphologies emerge from a finely tuned interplay of lipid composition, mechanical constraints, and physicochemical environmental conditions.

Lipid molecules contribute to membrane mechanics through their properties such as intrinsic shape parameter (affecting spontaneous curvature), melting temperature (determining rigidity), tilt, and hydrocarbon tail lengths (that affect bilayer thickness).[4] Concurrently, a consequence of the fluid nature of the membrane is that the components that prefer certain localities with specific mechanical properties (such as curvature, thickness or rigidity), demix or phase separate to form regions that are rich in one or another of the components.[5] The coupling of the dynamics of these mixing-demixing processes and the changes in the mechanical properties of the membrane, have been shown to give rise to pattern formation in phase separation and consequently, complex morphologies of the assemblies.[6]

Received: July 28, 2025
Revised: October 29, 2025
Accepted: November 12, 2025
Published: November 24, 2025

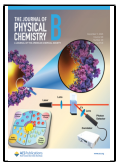

ACS Publications

© 2025 American Chemical Society

In protein-free vesicles, pattern formation has been observed in membranes undergoing phase separation between liquid-ordered (L_o) and liquid-disordered (L_d) domains. Using phase-selective fluorescent labeling and high-resolution fluorescence microscopy, Baumgart et al. (2003) illustrated how the coupling of membrane curvature to line tension at phase boundaries explains such complex morphologies.[5] Computational models further elucidate that elastic deformation of the membrane and phase separation of the lipids cooperatively drive such pattern formation.[7]

Membrane protein-containing lipid assemblies have also been shown to exhibit pattern formation, owing to the coupling of membrane curvature dynamics and liquid−liquid phase separation into protein rich and lipid rich regions. These proteins often preferentially associate with membrane regions of specific curvature and, in turn, deform the membrane locally. The mechanical coupling of such proteins was shown to induce two kinds of phase separating instabilities: Cahn Hillard and Turing instabilities. Cahn-Hillard instability is introduced when small fluctuations lead to demixing of the components to create dense and dilute regions that grow with time (Ostwald ripening). Turing instability is introduced when the diffusion rates of the two components differ and leads to stable-pattern formation with preferred length scales.[6]

Physical parameters such as temperature, pressure, and mechanical forces also play significant roles in modulating membrane behavior. For instance, the interplay of temperature change induced phase change and arrested order and topological defects can result in 'crumpled' morphologies in single component vesicles.[8] The application of localized mechanical perturbations via optical traps or micropipette aspiration has been used to stretch vesicles from spherical to prolate, tubular, or pearls-on-string shapes, revealing the mechanical response of membranes to point forces.[9,10] Additionally, bulk mechanical stimuli such as shear flow, especially when combined with thermal cycling, have been shown to transform spherical vesicles into complex, anisotropic structures. This phenomenon, studied in DPPC vesicles, has intriguing implications for protocell models in hydrothermal vent environments, where dynamic thermal and fluid conditions may have influenced early membrane evolution.[11]

A molecular dynamics simulation-based study by Bansal and Mittal (2013) reported curvature preference of component lipids in apparently flat lipid bilayers to give rise to kinetic windows of momentary destabilization in their distribution, which can lead to the genesis of complex geometries.[12] These findings suggest that membrane transformations, especially in protein-free systems, may not require continuous driving forces but instead can arise from short-lived energy inputs, offering a compelling framework to interpret spontaneous remodeling events in experimental setups and natural environments alike.

In this work, we have captured rare and apparently spontaneous membrane remodeling events in giant unilamellar vesicles (GUVs) composed of lipids with (POPC:DPPC) and without (POPC:DOPE) the tendency to phase separate into liquid disordered (L_d) and solid/gel (S) phases at room temperature. Quantitatively, these events occurred in approximately 6% of POPC:DOPE vesicles and 2% of POPC:DPPC vesicles on Day 1 across multiple independent preparations, confirming their rarity in otherwise stable vesicle populations. These events were captured under isothermal and chemically unperturbed conditions using real-time confocal microscopy. Unlike prior studies that have reported such morphological transitions as static snapshots, our time-resolved imaging enables a quantitative assessment of the temporal evolution of remodeling. In a systematic study of these events, we integrate 2D/3D geometric analysis with curvature energy calculations and delineate the role of intrinsic lipid properties (shape parameter and phase behavior) and extrinsic mechanical perturbations (laminar flow and minor evaporation induced osmotic changes) in driving these transitions.

These morphological transformations were observed to fall under two categories: energetically neutral transformations and energetically dissipative transformations. Energetically neutral transitions, which do not show significant changes in total membrane elastic energy, were primarily observed in POPC:-DOPE (9:1) vesicles. Energetically dissipative transitions, which show a decline in elastic energy over time, were observed in POPC:DPPC (9:1) vesicles. To our knowledge, this study is among the first to report dynamic membrane remodeling events under stable temperature and chemical conditions in binary, protein-free lipid membranes devoid of cholesterol or sphingomyelin.

METHODS

Chemicals. The lipids POPC (1-palmitoyl-2-oleoyl-*sn*-glycero-3-phosphocholine), and DPPC (1,2-dipalmitoyl-*sn*-glycero-3phosphocholine), as well as the probe 18:1 Liss Rhod PE (1,2-dioleoyl-*sn*-glycero-3-phosphoethanolamine-*N*-(lissamine rhodamine B sulfonyl) (ammonium salt)) were procured from Avanti polar lipids.

Vesicle Preparation. GUVs composed of POPC:DOPE at (9:1) and POPC:DPPC at (9:1), (8:2) and (1:9) molar ratios were prepared using the gentle hydration protocol (as described by Kubsch et al.).[13] Lipid films were labeled using 1/1000 (mol/mol) of the L_d phase specific probe Liss Rhodamine PE, a concentration that has been established to show negligible dye-induced membrane alteration or oxidation under standard fluorescence imaging conditions.[14,15] 100 mM sucrose solution containing 50 mM KCl at pH 7.0 was used as the aqueous phase for hydration, following established literature protocols which optimize GUV yield and stability while preserving physiologically relevant, yet experimentally tractable, conditions.[5,16] The detailed stepwise protocol is available in the Supporting Information. DPPC is a symmetric lipid with two saturated 16-C palmitoyl tails, a phosphatidylcholine head and a melting temperature (Tm) of ∼41 °C. DOPE is symmetric with two 18-C unsaturated oleoyl tails, a phosphatidylethanolamine head and a Tm ∼−16 °C. While POPC is asymmetric with one saturated palmitoyl tail and one unsaturated oleoyl tail with a phosphatidylcholine head. Here, gentle hydration was chosen over electro-formation since several studies have suggested the possibilities of artifacts (such as asymmetric lipid distribution and lipid oxidation in case of electroformed vesicles).[17−20]

Furthermore, gentle hydration mimics natural vesicle formation more closely compared to electro-formation, making it a suitable model for studies exploring lipid membrane behavior in prebiotic environments and the origins of life. Most important for our study is the assumption of unilamellarity of the GUVs—this is confirmed by (a) replication of earlier protocols for preparation of GUVs that assume unilamellarity based on fluorescence distributions in the vesicles,[21,22] (b) observations of rare morphological unilamellar transitions confirmed by electron-microscopy data published much earlier than this work[23,24] and (c) DIC observations of our vesicles.[25] Thus, while other techniques based on gentle hydration such as

https://doi.org/10.1021/acs.jpcb.5c05220
J. Phys. Chem. B 2025, 129, 12702−12714

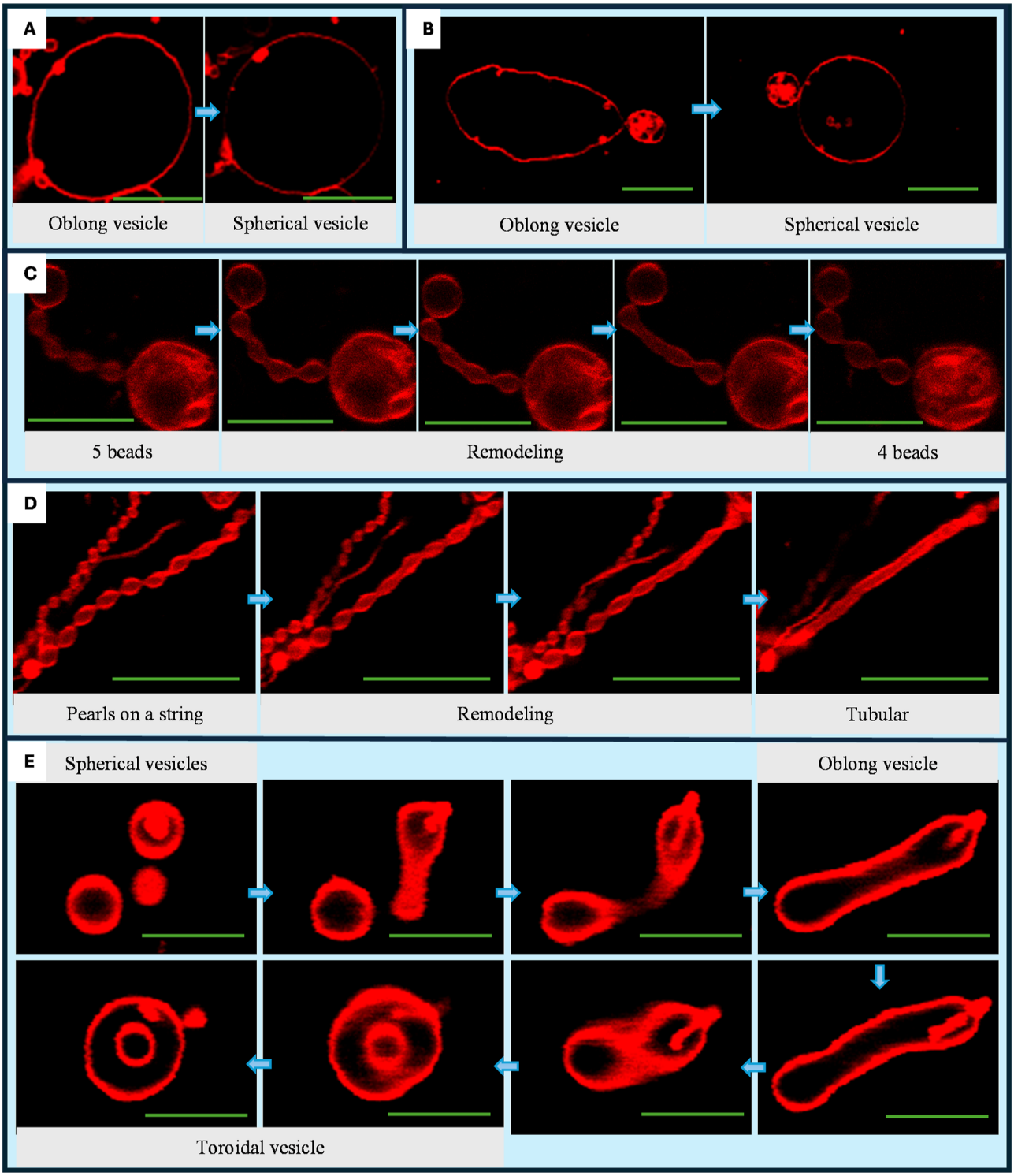

Figure 1. Representative frames of confocal microscopy images (Liss-Rhodamine PE channel) of the membrane remodeling events (A–E) selected for further geometric and energetic analyses. (see Supporting Information documents for all frames including the DIC channel images). Green bar represents 10 μm in all frames.

PAPYRUS[26], may provide a larger fraction of unilamellar vesicles compared to our method, our single-vesicle-observational approach (specifically observing GUVs only) overcomes the requirement of more GUVs compared to possible GMLVs.

For long-term observations, samples were aliquoted into multiple sterile, opaque, brown microcentrifuge tubes, sealed with parafilm, and stored at 27 °C. These precautions were taken to minimize potential confounding factors such as evaporation, microbial contamination, photodegradation, and lipid or dye degradation during storage.

Imaging. These vesicles were studied and recorded over extended periods of time under Olympus FV1200 (Photometrics Evolve Delta) confocal microscope at room temperature, using a 543 nm laser with a measured on-stage power consistently below 0.2 mW (using a Gentech Eo power meter) and a 100× oil immersion objective. This laser power is well

https://doi.org/10.1021/acs.jpcb.5c05220
J. Phys. Chem. B 2025, 129, 12702–12714

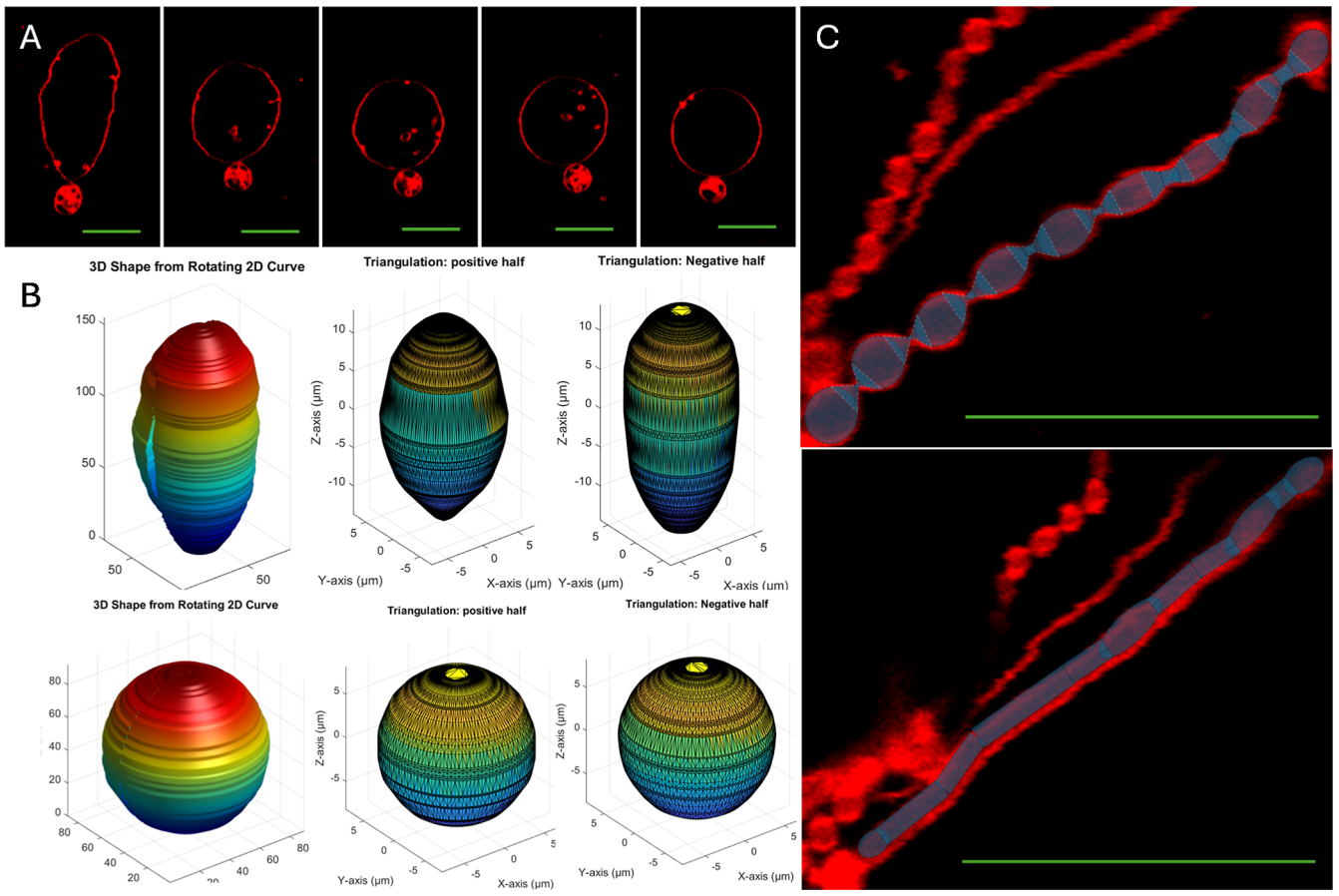

Figure 2. Quantitative analysis of axisymmetric (A,B) and nonaxisymmetric (C) remodeling events. (A) Reference confocal frames of event-2. (B) 3D projections generated using semiautomated MATLAB based algorithm (see Supporting Information for the algorithm). 3D projections created by rotating the 2D shape by 180° (left); the boundary was divided into left (negative) and right (positive) halves and rotated by 360° and triangulated meshes were created of the two-halves (center and right). The energies were calculated for both halves and averaged to give the energy of the whole. (C) non-axisymmetric assemblies were divided into ellipsoidal sections, triangular sections, and cylinders to calculate the geometric and energetic parameters. Green bar represents 10 μm in all frames. (see Supporting Information for for further details).

below the threshold for pronounced oxidation effects as reported in previous studies that observed dramatic transitions at $\geq$ 0.38 mW and much higher dye content.[27] The softwares used for the recordings were Fluoview and Olympus cellSens Dimension 1.9 (2009−2013). In addition to confocal fluorescence imaging, differential interference contrast (DIC) images were simultaneously recorded to enhance contrast and reveal membrane contours. Epifluorescence imaging of the same samples was also performed independently. Samples were first imaged approximately 2 hours after completion of the hydration step (Day 1), followed by additional sessions on Days 3 and 9. Across 10 independent preparations for POPC:DOPE (9:1) and 6 for POPC:DPPC (9:1), a total of 122 and 578 vesicles, respectively, were catalogued on day 1 based on morphological classification from time-lapse confocal imaging. If vesicle yield remained sufficient, additional imaging sessions were carried out between three and four weeks after preparation. When including all observation days, 140 POPC:DOPE and 1086 POPC:DPPC vesicles were examined. No deliberate physicochemical perturbations (e.g., osmotic shock, temperature shifts, or pH changes) were introduced at any stage of the experiment. All comparative observations between preparations with different compositions were made using preparations from day 1 ensuring consistency across samples and excluding compositional changes due to storage. Further observations on long-term behavior were made separately.

Aside from the known phase separation behavior of POPC:DPPC mixtures at room temperature and the shape parameter mismatch between POPC and DOPE, the system remained chemically and thermally unaltered. Vesicles without visible phase separation were therefore expected to maintain stable morphologies over time. While most assemblies were observed to be seemingly stable and unchanging in the time course of observation, several others were observed to be undergoing substantial changes in their morphologies. These spontaneous remodeling events formed the focus of further investigation. The gentle hydration method inherently produces a heterogeneous vesicle population comprising unilamellar, multilamellar and vesicles with internal membrane fragments. Hence, for kinetic analyses, only the vesicles displaying clearly resolved outer membranes with static internal structures were selected from Day 1 preparations to ensure that the observations reflected intrinsic membrane behavior, independent of potential storage-related alterations. Figure 1 displays representative time-resolved image sequences of the remodeling events selected for quantitative analysis.

Geometric Analysis. To quantitatively characterize the observed remodeling events, a geometric analysis pipeline was developed. Two-dimensional parameters, including enclosed

https://doi.org/10.1021/acs.jpcb.5c05220
J. Phys. Chem. B 2025, 129, 12702−12714

Table 1. GUV Morphologies Observed at Varying (Liquid Disordered:Solid/L_d:S) Phase Specific Lipid Ratios

composition	observed morphologies, shape transitions and phase behavior	literature sightings of similar morphologies
10:0 (L_d:S phase ratio) {POPC:DOPE (9:1) compositional ratio}	stable morphologies: spherical, prolate, tubular, pearls on string	Bilayer asymmetry.[23] DPPC vesicles in shear force with temperature cycling.[11 28 11 29]
	shape transitions: (1) slack, irregular, prolate to spherical firm vesicle. (2) Pearls on string morphology with transient, minor shape changes	(1) Vesicles with PEG-lipids.[28] DPPC vesicles cooling from above Tm temperatures.[11] (2) DMPC:DGDG vesicles with laser tweezers[29]
9:1 (L_d:S) {POPC:DPPC}	stable morphologies: (1) spherical firm vesicles without visible solid domains. (2) Spherical slack, fluctuating vesicles without visible solid domains. (3) Spherical vesicle exhibiting a single circular, triangular or bar-shaped solid domain	Various shapes of L_o domains in L_d–L_o phase-separating vesicles.[5] ;o Ternary vesicles under osmotic pressure stress: tubes, pearling, oblong vesicles.[30 29 10 31]
	shape transitions: (1) Pearls on string morphology with changing the sizes and number of "beads". (2) Pearls on string to tube morphology. (3) Three vesicles, possibly connected, transitioning to form a single oblong vesicle which folds on itself to give a final apparently stable toroidal shape	(1) DMPC:DGDG vesicles with laser tweezers.[29] (2) Pearling under the effects of external uniform force.[10] (3) DLPC:DPPC giant vesicles[31]
8:2 (L_d:S) {POPC:DPPC}	morphologies: (1) Phase separated vesicles exhibiting solid phase with webbed or multistriped shapes. (2) Clusters of small multilamellar and indiscernible assemblies	(1) GUVs with L_o–L_d phase separation.[5,7] (2) DLPC:DPPC giant vesicles[31]
1:9 (L_d:S) {POPC:DPPC}	morphologies: clustered, indiscernible assemblies	-

Table 2. Correlation of Geometric and Energetic Parameters With Time for Selected Events A to E[a]

event	composition	initial	final	time (s)	parameter	Pearson's r	asymptotic/nonasymptotic
A	POPC:DOPE (9:1)	flaccid prolate	firm spherical	100	surface area	NC	
					volume	NC	
					circularity	0.79	non-asymptotic
					E	NC	
					E_d	NC	
B	POPC:DOPE (9:1)	flaccid oblong	firm spherical	58	surface area	−0.87	asymptotic
					volume	−0.71	non-asymptotic
					circularity	0.70	asymptotic
					E	NC	
					E_d	NC	
C	POPC:DPPC (9:1)	5 pearls on string	4 pearls on string	108	surface area	NC	
					volume	0.36	non-asymptotic
					E	−0.31	asymptotic
					E_d	−0.30	asymptotic
D	POPC:DPPC (9:1)	pearls-on-string	tube	65	surface area	−0.53	non-asymptotic
					volume	−0.58	non-asymptotic
					E	−0.72	non-asymptotic
					E_d	−0.51	asymptotic
E	POPC:DPPC (9:1)	spherical to oblong vesicle	toroidal	36	surface area	NC	
					volume	NC	
					E	−0.87	asymptotic
					E_d	−0.69	asymptotic

[a]Pearson's correlation value for statistically significant ($p \leq 0.05$) correlations are summarized here. Parameters marked NC (no correlation) had a p-value >0.05 for the two tailed t-test, and hence any correlation was concluded to be statistically insignificant.

area (a) and perimeter (p) were extracted using a semi-automated MATLAB-based algorithm. Circularity (C) was calculated using the standard formula

$$C = 4\pi a/p^2 \quad \text{(i)}$$

For vesicles exhibiting apparent rotational symmetry, a custom MATLAB algorithm was designed/created to estimate three-dimensional parameters: surface area (A) and volume (V) using the boundary coordinates (see Supporting Information for details). For non-axisymmetric vesicles, geometrical approximations were employed by segmenting the shape into ellipsoidal, conical, and cylindrical regions; the 3D parameters were then computed for each section and summed to obtain total surface area and volume (Figure 2c). Pearson's correlation coefficients (r) were calculated for all geometric parameters as a function of time. The statistical significance of these correlations was assessed using a two-tailed t-test and the p-values were calculated.

The geometric analysis was aimed at addressing the possible interactions of defects, internal inclusions, or other assemblies with the assembly being studied. Additionally, where possible, geometric parameters of adjacent vesicles within the same field of view were tracked across the time series to check for any interactions with the assembly of interest.

Elastic Energy Calculations. In order to investigate the cause of these shape changes, the elastic energies of the assemblies were calculated for each frame. The Canham-Helfrich model describes the elastic energy (E) of the membrane in terms of an energy density that is a function of the local shape of the membrane:

https://doi.org/10.1021/acs.jpcb.5c05220
J. Phys. Chem. B 2025, 129, 12702−12714

$$E = \frac{k}{2}\int_0^A (C_1 + C_2 - C_0)^2 \partial A + k_G \int_0^A C_1 C_2 \partial A \quad \text{(ii)}$$

here, k is the bending rigidity (typically ∼20 k_BT for lipid bilayers), C_1 and C_2 are the principal curvatures (inverse of local radii), C_0 is the spontaneous curvature (typically ∼0 μm^{-1} for symmetric lipid bilayers), and k_G is the Gaussian bending rigidity. This energy density is then integrated across the entire surface of the vesicle to get the total elastic energy of the membrane.[4] For remodeling events that did not involve changes in topology (i.e., constant Euler characteristic; Events A-D), the Gaussian curvature term was excluded from the analysis.

For axisymmetric vesicles, 3D surface meshes were generated by rotating boundary profiles and triangulating the resulting shape using MATLAB functions (Figure 2). Principal curvatures (C_1, C_2) were computed across the mesh, and local energy densities (∂E) were integrated to yield total elastic energy (E). Energies from the left and right halves were computed separately and averaged to account for any asymmetries. Although this method does not give the exact 3D geometry of the assembly, it gives as close a contour as possible within the resolution limit of a confocal system.

For non-axisymmetric assemblies, elastic energies of the geometrically defined sections (ellipsoidal, conical, tubular) were calculated individually and summed up to obtain the system's total energy. Representative methodology for both axisymmetric and nonaxisymmetric reconstructions used for geometric and energetic calculations is presented in Figure 2.

Average energy density ($E_d = E/A$) was also computed to normalize energy values across vesicles with varying surface areas. To assess energetic trends over time, Pearson's correlation coefficients (r) were calculated for energy vs time values, and their statistical significance was checked using the p-value (from the t-statistic). Transitions in which the energy-time trajectory approached a plateau were interpreted as transitions reaching a semistable or metastable end point.

Table 2 summarizes the statistically significant (p-value ≤0.05) correlations of both geometric and energetic parameters with time for the selected five shape transition events, to highlight meaningful trends during remodeling, along with the observation of asymptotic behavior of the curve.

OBSERVATIONS

Throughout the course of imaging, differential interference contrast (DIC), confocal, and epifluorescence microscopy revealed no evidence of microbial contamination in any of the samples.

Composition-Dependent Morphologies. Table 1 summarizes the observed morphologies in different L_d:S compositions and the representative frames are compiled in Figures S10 (POPC:DPPC) and S11 (POPC:DOPE).

The POPC:DOPE (9:1) preparation has both the constituent lipids in the L_d phase at room temperature and hence effectively represents a (10:0) L_d:S ratio. Most vesicles in this preparation displayed nearly spherical morphologies. A subset displayed oblong, flaccid, and dynamically fluctuating shapes. Tubular assemblies, along with some vesicles exhibiting pearls-on-a-string morphologies were observed as well. 27% (33 out of 122) of these assemblies on day 1, and 25% (35 out of 140) across all days of observation, exhibited non-spherical morphologies. 5.73% (7 out of 122) of assemblies observed on day 1, and 7.14% (10 out of 140) assemblies across all days were found to undergo morphological changes.

Two major kinds of shape transitions were observed in this composition: (1) flaccid, fluctuating vesicles transforming into spherical, taut vesicles, and (2) pearls-on-string assemblies transiently changing their structures before reverting to their initial morphology. While the first type of transition was sufficiently well recorded for image analysis, the latter lacked adequate resolution or temporal coverage for further quantification.

In the POPC:DPPC (9:1) mixture, most vesicles, including the remodeling assemblies, appeared uniform in fluorescence intensity, indicating an absence of visibly segregated solid domains. This is in line with the observations in (POPC:DPPC) binary lipid membranes, that suggest that the membrane predominantly exhibits the liquid disordered (L_d) phase at physiological temperatures at such low DPPC concentrations.[32] However, static vesicles within the same preparation showed increasing evidence of phase separation over time. In day 1 vesicle preparations of this composition, only ∼1.4% (8 of 578) of the assemblies exhibited distinct dark regions indicative of solid domains. This fraction rose modestly to ∼2.3% by day 3 and ∼11.5% by day 9, reaching a peak of ∼44.9% (70 of 156) by day 16. Subsequently, the proportion declined to ∼9.3% by day 18, while by day 27, ∼33% (1 of 3) of the remaining assemblies exhibited a single, well-defined solid region. This decline can possibly be explained by a reduction in the number of remaining vesicles in the sample that could be observed. Among the dynamically remodeling vesicles in this composition, various transitions were captured; most notably, changes in bead number and shape in pearls-on-string morphologies (event-C), transitions from pearls-on-string to tubes (event-D), and rare folding of oblong vesicles into toroidal structures (event-E). Notably, prolate ellipsoidal vesicles were also observed but remained morphologically static during imaging, except for minor (possibly thermal) fluctuations. Such long-term evolution of slow equilibration of the solid phase has been observed in compositions with higher DPPC concentrations (30−50%).[33] The observed frequency of occurrence of shape transformations is 1.7% on Day 1 (10 out of 578 vesicles) and 1.1% across all days (12 out of 1086 vesicles).

Increasing the DPPC content to POPC/DPPC (8:2) resulted in a lower yield of GUVs overall. Most observed assemblies (66.7%) exhibited evident L_d−S phase separation, frequently in the form of striped or webbed domains. The assemblies could only be imaged using epifluorescence microscopy. When reimaged on day 3, the sample consisted predominantly of aggregated or indistinct vesicle clusters, precluding meaningful geometric analysis.

At the highest DPPC content, POPC/DPPC (1:9), the lipid assemblies appeared small, densely clustered, and optically unresolved. No individual vesicle structures could be reliably identified, likely due to the formation of multilamellar or aggregated assemblies dominated by the solid phase.

For further quantitative analysis, only the remodeling events from day 1 of preparation with clearly recorded transitions, well-focused frames capturing the equatorial plane and minimal interference from neighboring vesicles were selected. While many other shape remodeling events were noted, only five events met these criteria for further analysis. These five events encapsulate the predominant remodeling patterns observed: transitions involving changes in vesicle sphericity, pearls-on-string morphologies with varying bead numbers or progression to tubular structures, and the rare and complex toroidal transformation (event E).

https://doi.org/10.1021/acs.jpcb.5c05220
J. Phys. Chem. B 2025, 129, 12702−12714

Quantitative Analysis of Remodeling Events. The selected five membrane remodeling events (labeled A through E) were analyzed and are presented in order of increasing complexity of morphological transformation (Figure 1). Events A and B were observed in POPC/DOPE (9:1) vesicles, and events C, D, and E occurred in POPC/DPPC (9:1) assemblies. Correlation analysis of geometric and energetic parameters with time for these five shape transitions is summarized in Table 2.

Event A: Flaccid to Spherical Transition. A vesicle initially exhibiting a prolate, flaccid morphology was observed to transition into a nearly spherical, taut form in ∼100 s. Three-dimensional geometric parameters—surface area (A) and volume (V)—showed no significant correlation with time, suggesting conservation of vesicle material. An increase in circularity and notable changes in 2D parameters (area, perimeter) substantiated the morphological transformation. Both total elastic energy (E) and energy density (E_d) remained statistically constant throughout the transition, indicating that the initial and final configurations exist at similar energetic levels. Additionally, adjacent vesicles within the same field of view that could be tracked showed no changes in geometric parameters, supporting the interpretation that such inclusions are static and do not actively participate in membrane transformations.

Event B: Oblong-to-Spherical Transition. The vesicle transformed from an oblong, flaccid structure to a stable spherical form within ∼58 s. Geometric parameters showed a slight decrease in 3D (A, V) and 2D (p, a). The circularity increased with time and reached an asymptote. The total elastic energy as well as the E_d of the assembly remained unchanged in the timespan of the shape transition. A smaller adjacent vesicle, initially suspected of interacting with the remodeling event, exhibited no statistically significant geometric or energetic changes.

Event C: Pearls-on-String Morphology Transition. This POPC/DPPC assembly initially displayed a pearls-on-string morphology, consisting of a larger terminal bead, four uniform intermediate beads, and a multilamellar assembly at the other end.

Remodeling was observed over ∼108 s, primarily involving the central beads and larger terminal bead. Quantitative analysis revealed no changes in the "A, p, and a"; a minor increase in V; and a net decrease in A/V and p/a. Total elastic energy (E) and E_d were observed to decrease over time, tending toward an asymptote. These trends suggest a spontaneous relaxation toward a lower-energy state. Since the terminal multilamellar assembly showed no significant geometric or energetic changes, it was concluded to be a nonparticipating component.

Event D: Pearl-to-Tube Remodeling. In this event, a longer pearls-on-string assembly transitioned into a tubular structure over 65 s. Analysis was focused on the remodeling region. A, V and p decreased over time, indicating some shrinking in the assembly. E as well as E_d were observed to decrease over time, again tending toward an asymptote. These results support a model of energetically driven relaxation following a perturbation or instability.

Event E: Vesicle Fusion and Toroidal Transformation. Initially, three spherical vesicles were observed in proximity. The DIC images showed them right next to each other and could not resolve whether they were connected at this point. At 5.2 s time frame, two vesicles apparently merged and a connecting tube to the third was observed. By 6.8 s (next frame), all three appeared to form a single oblong vesicle, which then relaxed over the following ∼20 s. At 22.1 s, the vesicle folded onto itself, and the ends fused, ultimately adopting a stable configuration resembling either a toroidal structure or a sphere-within-a-sphere geometry. At this point, the fusion cost of $4\pi\kappa$ (359.4 k_BT) was added to the calculations.[34] The final morphology remained unchanged until the end of the recording (38.8 s). The irregular internal structure could be tracked throughout the transition, acting as a physical marker of the membrane locality, and was observed to be unchanging throughout the transition.

Geometric analysis supported the toroidal geometric interpretation: the surface area and volume of the toroidal final state matched the preceding structures in all timeframes. Furthermore, a high correlation between the trajectories of inner and outer circular centroids indicated mechanical continuity (Pearson's coefficient = 0.97 for x-coordinates and 0.64 for y-coordinates), which would be inconsistent with independent internal motion in an encapsulated sphere. This folding of the vesicle to form toroidal assembly is reminiscent of the discocyte−stomatocyte transitions, as observed by Berndl et al. (1990).[23]

The 3D geometric parameters showed no correlation with time, suggesting that all the lipids as well as the enclosed volume were accounted for.

The total elastic energy exhibited a strong negative correlation with time and plateaued after approximately 25.6 s, indicating asymptotic behavior. Given the high energetic cost typically associated with membrane fusion, we hypothesize that the vesicles involved may have been pre-connected via sub-resolution nanotubular structures prior to the onset of observable fusion. This interpretation is supported by DIC imaging, which revealed a single visible interconnecting tube. Such a configuration would render the initial stages of the remodeling event analogous to a pearls-on-string-to-tube transition, rather than representing de novo fusion of initially separate vesicles.

The consistency between trends in average elastic energy density (E_d) and total elastic energy (E) was taken as additional support for the robustness of the observed energy−time correlations.

DISCUSSION

Compositional Influence on Morphology and Phase Behavior. The spontaneous morphological transitions observed in protein-free GUVs across varying lipid compositions underscore the intricate role of membrane composition in modulating mechanical stability, shape dynamics, and pathway accessibility. In both POPC:DOPE and POPC:DPPC (9:1) mixtures, we found that while most vesicles retained near-spherical shapes indicative of mechanical stability, a minority exhibited pronounced remodeling events—often transient but occasionally leading to persistent transformations.

POPC:DOPE (9:1) vesicles, composed entirely of lipids in the L_d phase at room temperature, presented with flexible, dynamic geometries: flaccid, oblong, tubular, and rarely pearls-on-a-string morphologies. These shapes likely emerge from reduced membrane tension, enhanced thermal fluctuations, and the intrinsic negative spontaneous curvature conferred by DOPE. While the majority of vesicles remained spherical, a subset underwent visible transitions: notably, flaccid shapes reforming into taut spheres, and pearls-on-a-string structures transiently reorganizing. These observations are consistent with earlier reports indicating that DOPE, owing to its small headgroup and unsaturated tails, promotes non-bilayer tenden-

https://doi.org/10.1021/acs.jpcb.5c05220
J. Phys. Chem. B 2025, 129, 12702−12714

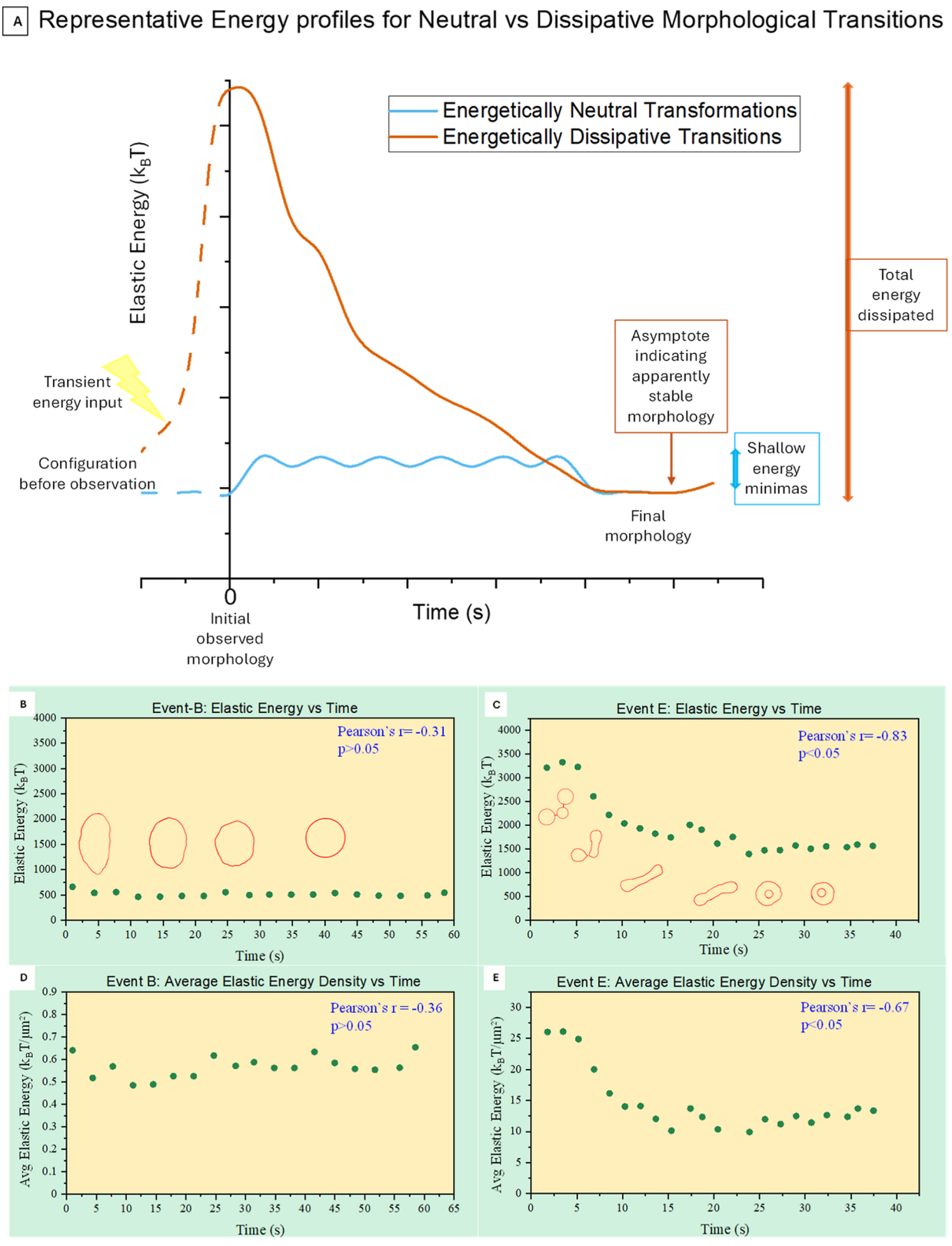

Figure 3. Hypothetical and experimental energy landscapes for GUV morphological transitions: (A) expected hypothetical energy evolution during remodeling events. Energetically dissipative transitions (red) exhibit a decline in total elastic energy tending toward an asymptote, while energetically neutral transitions (blue) occur across shallow energy minima. The dashed section represents a hypothesized transient elevation in energy due to external perturbations during sample preparation. Deviations from ideal behavior are expected due to the complex interplay of curvature-driven stress, heterogeneous relaxation kinetics, local lipid packing, and potential mechanical instabilities. (B,C) show experimentally derived total elastic energy vs time plots for events B (energetically neutral) and E (energetically dissipative), respectively (with traces of morphologies at different time points). (D,E) present corresponding changes in average elastic energy density (E_d) for events B and E.

https://doi.org/10.1021/acs.jpcb.5c05220
J. Phys. Chem. B 2025, 129, 12702−12714

cies and negative curvature stress, especially under low-tension conditions.[12,35−37]

In the POPC:DPPC (9:1) system, vesicles displayed a diverse array of morphologies indicative of mechanical heterogeneity, including oblong and rod-like forms, tubular structures, toroidal topologies, and pearls-on-string assemblies. Consistent with established phase diagrams and prior reports, none of the remodeling vesicles in this composition exhibited detectable phase separation under fluorescence microscopy, as the low (10%) concentration of DPPC is below the threshold typically required for optically resolvable domain formation.[32] However, nanoscale compositional fluctuations and transient submicron domains can occur even at such low solid-lipid fractions, which are often below the resolution limit of conventional confocal imaging. Over extended incubation, a larger fraction of vesicles began to develop visible phase-separated domains, a phenomenon that becomes more pronounced with increasing DPPC content and prolonged sample aging.[33,38] These domains adopted diverse geometries-circular, star-like, triangular, and bar-shaped, remarkably similar to those reported in prior studies on phase-patterned GUVs (Figure S11).[5,6,30]

The delayed appearance of such phase-separated features points to possible kinetic trapping and metastability immediately after vesicle formation, consistent with prior work on slow thermotropic lipid demixing.[38,39] Dynamic transitions in this composition, including pearls-on-string rearrangements and the rare folding of oblong vesicles into toroidal shapes, underscore the capacity of phase-heterogeneous membranes to generate internal mechanical stresses sufficient to drive large-scale remodeling, even in the absence of proteins or external stimuli. These findings reinforce theoretical predictions that local curvature and composition are tightly coupled, enabling feedback-driven access to metastable morphologies.[31,40]

High DPPC Content Vesicles: Aggregation and Reduced Vesicle Yield—At higher DPPC ratios (POPC:DPPC = 8:2 and 1:9), vesicle yield was significantly reduced. The few vesicles that formed displayed clear solid-phase separation, often as striped or web-like patterns, in agreement with prior studies on gel-phase-enriched membranes.[5,7] These structures were mechanically rigid, consistent with known effects of gel-phase enrichment, including line tension in separated phases, reduced membrane fluidity and increased bending rigidity.[7,31,41−43]

Taken together, these findings emphasize that even modest changes in the liquid-to-solid lipid ratio can dramatically alter the membrane's curvature landscape, fluctuation dynamics, and remodeling potential. This compositional control, independent of protein scaffolds, highlights an intrinsic capacity of lipid bilayers to undergo complex morphological transformations via internal reorganization alone.

Mechanistic Classes of Remodeling Events. The observed remodeling events fall into two categories: (i) events where total elastic energy (and energy density E_d) remain unchanged, and (ii) events associated with a decline in elastic energy, often approaching an asymptote. The latter were particularly notable in POPC:DPPC assemblies, with POPC existing in the L_d phase and DPPC in the S phase. All transitions were observed under isothermal, chemically unperturbed conditions. Figure 3 illustrates the hypothetical energy vs time profiles for these two classes of morphological transitions, along with the corresponding experimentally derived energy parameters plotted against time for each case.

Energetically Neutral Transformations. These were observed in POPC/DOPE vesicles, where the Tm of both the component lipids is below the observed temperature and no phase separation is anticipated. The absence of significant energy gradients during remodeling suggests that these assemblies occupy shallow local minima in the energy landscape. In landscapes like these, even subtle perturbations such as minor mechanical perturbations, thermal noise, or stochastic lipid asymmetries may drive transitions between quasi-stable morphologies. These transformations possibly remain reversible and dynamic, unless stabilized by external interactions. In cellular contexts, such stabilizing factors may include membrane-associated proteins or cytoskeletal scaffolds that locally reinforce curvature or constrain lipid mobility.

In this binary lipid composition, these varying morphological states occupying the shallow minima in the energy landscape are possibly arising due to the difference in the shape parameters of the two lipids. The conical geometry of DOPE imparts a strong negative spontaneous curvature, while POPC favors flatter bilayers. This intrinsic mismatch creates internal curvature stress that can destabilize symmetric configurations and promote dynamic remodeling, even in the absence of visible phase separation.

Simulations and experimental studies show that even in flat bilayers, conical lipids can induce local packing defects that mimic curvature stress, enhancing the membrane's responsiveness to external or internal perturbations.[12,23,34,35]

Bansal and Mittal (2013) demonstrated that curvature asymmetries can emerge even in flat, symmetric bilayers due to differential leaflet arrangements of conical lipids, producing "kinetic windows" for spontaneous shape transitions.[12] Mittal and Chauhan (2022) further proposed that protein-free membranes often undergo transformations not by global energy minimization, but via transiently accessible metastable states stabilized by kinetic traps.[44]

Our findings support this framework: in the absence of external energy gradients, the observed remodelings in POPC:DOPE vesicles likely reflect internal fluctuations around low-energy plateaus, governed by spontaneous curvature, lipid geometry, and stochastic asymmetries.

Energetically Dissipative Remodeling. In contrast, vesicles composed of POPC:DPPC (9:1) showed transitions accompanied by a decrease in total elastic energy tending toward an asymptote, consistent with barrier-limited relaxation from higher-energy configurations, suggesting a slow and progressive relaxation into a stable low-energy configuration following transient mechanical perturbation.

These vesicles exhibited a wide range of nonspherical shapes: rod-like, tubular, toroidal, and pearls-on-string morphologies. Although the DPPC fraction is below the threshold typically associated with visible phase separation, as confirmed by established phase diagrams,[32] the two lipid components inherently tend to segregate due to distinct properties such as membrane stiffness, thickness, and curvature41, 45 In our experiments, remodeling vesicles did not exhibit resolvable phase-separated domains at the confocal imaging scale, likely reflecting the low (10%) abundance of DPPC. However, nanoscale gel domains or transient compositional fluctuations occurring below the resolution limit of confocal microscopy may still be present, in line with reports of submicron heterogeneity in such systems. Thus, while classical coexisting phases were not directly observed at this ratio, the formation of distinct dynamic morphologies and energy dissipation behaviors are plausibly influenced by local compositional heterogeneity and the intrinsic biophysical differences between the two lipid species.

https://doi.org/10.1021/acs.jpcb.5c05220
J. Phys. Chem. B 2025, 129, 12702−12714

The pronounced decrease in elastic energy was unexpected, given that such energy minimization processes are typically spontaneous and should have occurred by the time imaging commenced. This suggests that the assemblies may have gained energy after their formation, possibly due to mechanical perturbation during sample handling, such as pipetting or coverslip placement, which introduced geometric complexities. These mechanical perturbations could have induced metastable morphologies, which then relaxed over time.

Mechanical perturbations, even low piconewton-range forces, are known to induce morphological transformations in lipid membranes.[9,11] Mechanically triggered pearling, as reported by Bar-Ziv and Moses (1994) and Vlahovska (2014), provides a compelling analogy. The former reported instability and "pearling" states produced in tubular membranes induced by the competition between membrane tension and bending rigidity, with increased tension promoting the pearling transition.[45] The latter study reported the induction of symmetry-breaking shape transitions, such as pearling of tubular vesicles and pear/dumbbell shaped vesicles, in the presence of an external uniaxial extensional flow. This was reported despite the flow being symmetric, suggesting intrinsic mechanical instabilities of the vesicle. The tendency of vesicles to undergo transition in external flow was linked to their reduced volume and higher aspect ratio, which explains why some vesicles in our samples exhibited complex morphologies while the others were stable.[10] Given the absence of applied flow in our setup, we posit that transient aqueous flow during sample preparation may act as an inadvertent extensional stress, leading to mechanical destabilization of high-aspect ratio vesicles.

Winter et al. (2025) showed that transient mechanical triggers can lead to instabilities in membranes undergoing liquid−liquid phase separation between lipids and proteins. The study suggests that transient external perturbations lead to Cahn-Hillard instabilities that cause disruption in the mixing of the components, leading to nucleation and growth of distinct phases via Ostwald ripening. Additionally, Turing instabilities arising from differences in component diffusion rates were shown to cause spatial pattern formation.[6] In our context, these mechanisms offer a plausible explanation for how small external perturbations could trigger phase rearrangements and morphological transitions in DPPC-containing vesicles.

In protein-free lipid bilayers, the coupling of membrane bending energy that favors smaller domains and lipid domain line tension (favors bigger domains) has been suggested to lead to arrested coarsening, giving rise to pattern formation.[5,7]

In 1987, Lentz et al. suggested that in SUV preparations, the rate limiting step of spontaneous fusion of small unilamellar vesicles may be the close juxtaposition of vesicle bilayers. In this study, we have captured and analyzed a remodeling event that involves folding of an oblong vesicle, followed by fusion of its ends to give a toroidal geometry. Here, the close juxtaposition of the ends caused by rapid folding (within 2−3 s) of the vesicle was observed to be followed by the fusion of the ends, supporting the relevance of this mechanism even in GUVs.[46]

Discocyte, stomatocyte, and toroidal morphologies have long been predicted as stable solutions in bending energy and area-difference elasticity models. However, direct experimental observation of an oblong vesicle folding over and fusing at its ends to form a stable toroid or sphere-within-a-sphere is exceedingly rare. Only a handful of studies, such as Berndl et al. (1987),[23] Seifert et al. (1991),[24] and Noguchi et al. (2015),[47] have captured comparable topological transitions, typically under highly controlled or simulated conditions. The infrequency of these events is attributable to their requirement for coordinated membrane and topological rearrangements and substantial energy barriers. Thus, the spontaneous observation of this transformation (event E) in our experiments adds a rare, experimentally validated example to the literature and further deepens our understanding of membrane shape transitions under minimalistic, protein-free conditions.

While every effort was made to minimize uncontrolled variables such as evaporation, lipid or fluorophore degradation, microbial growth, and minor compositional variance, we acknowledge that these factors cannot be entirely ruled out, particularly during prolonged imaging sessions. It is plausible that minor evaporation during imaging may have led to local changes in osmolarity, potentially influencing membrane tension. Nonetheless, the frequency, reproducibility, and compositional dependence of these events suggest that they represent genuine biophysical responses rather than artifacts of experimental variability. The remodeling pathways accessed are therefore still mechanistically relevant and deserving of more research, even if evaporation plays a role as a trigger.

Although vesicle-to-vesicle compositional variability is a recognized feature in GUV preparations, prior studies indicate this variability is typically confined within ±2−4 mol % of the bulk composition in binary lipid mixtures prepared by gentle hydration.[48] This narrow range of molar ratios (≈86:14−94:6 for 9:1 preparations) is insufficient to account for the distinct remodeling events observed here in ∼6% of POPC:DOPE and ∼2% of POPC:DPPC vesicles.

The potential for laser-induced photooxidation to induce morphological changes is effectively mitigated by employing low fluorophore (Liss-Rhod PE) concentrations (1/1000 mol/mol) and low on-stage laser power (0.2 mW).[14,15,27] Furthermore, the morphological transitions we observed are not accompanied by the hallmark features of photooxidation, such as rapid area expansion, catastrophic pore formation, or vesicle collapse that are observed at higher dye concentrations (≥1 mol %) and laser power (≥0.38 mW).[27] Liss-Rhod PE, used here at optimized concentrations, is among the most reliable reporters of L_d−S phase separations due to its high partitioning, small size and negligible interference with native systems.[5,49,50] While alternative, less photosensitizing dyes (e.g., Bodipy-PC or TopFluor cholesterol) could serve as additional controls to distinguishing intrinsic membrane remodeling from photo-oxidation-induced artifacts (which, as discussed above, are unlikely in our case), such probes (e.g., TopFluor cholesterol) may also lead to artifacts pertaining to probe-induced-phase/morphological-transitions.[51−53] Nevertheless, future studies employing different appropriate probes may further elucidate rare morphological transitions that are not reported while assuming stable GUV preparations.

Small occasional surface undulations observed in some assemblies do not significantly bias total envelope area/volume estimation given the spatial resolution of our confocal images (∼200 nm laterally), especially since the major transitions (prolate → sphere, pearls on string → tube) are associated with much larger deformations. Our main conclusions pertain to the energetic profile (e.g., presence/absence of plateau, relaxation time courses) and trend-wise changes, rather than absolute values. Therefore, small ambiguities from minor inclusions/defects do not undermine the validity of the mechanistic classification (shallow energy landscapes versus barrier-limited relaxation). Furthermore, the agreement of the elastic energy

https://doi.org/10.1021/acs.jpcb.5c05220
J. Phys. Chem. B 2025, 129, 12702−12714

density profile (E_d) with the total elastic energy (E) validates the observed trends in all the remodeling events.

Taken together, our observations point to a nuanced picture of membrane remodeling: while some assemblies sample multiple morphologies within flat energetic basins, others undergo progressive, energetically downhill shape transformations, possibly reflecting compositionally encoded pathways. This dichotomy highlights the importance of lipid composition in modulating both the shape dynamics and the energetic topology of membrane assemblies.

CONCLUSIONS

In this study, we have captured and systematically analyzed apparently spontaneous membrane remodeling events in giant lipid vesicles in the absence of any membrane proteins and without deliberate modulation of temperature, osmolarity, or pressure. Quantitatively, these remodeling events were rare, occurring in ∼6% of POPC:DOPE and ∼2% of POPC:DPPC vesicles on day 1 of preparation, underscoring the compositional dependence of membrane remodeling propensity. Real-time confocal imaging data was analyzed to retrieve geometric (3D and 2D) parameters and to calculate the elastic energy of the assemblies at each time point during remodeling, using a semiautomated MATLAB-based algorithm. Our observations suggest that the remodeling events fall under two categories: energetically neutral remodeling and remodeling characterized by a decline in elastic energy tending toward an asymptote. In POPC:DOPE vesicles, where both lipids are in the liquid-disordered phase but differ in intrinsic molecular shape parameters (cylindrical POPC vs conical DOPE), we observe energetically neutral remodeling events occurring over shallow energy landscapes. These reflect small fluctuations between quasi-stable membrane configurations driven primarily by curvature stress and molecular geometry differences.

In contrast, POPC:DPPC (9:1) vesicles composed of lipids differing sharply in melting temperature (with DPPC being a S-phase component and POPC being a L_d-phase component) exhibited energetically dissipative remodeling events, characterized by a measurable decline in total elastic energy tending toward an asymptote. This behavior suggests barrier-limited relaxation from transient, higher-energy states, possibly influenced by slowly evolving nanoscale solid domains below optical resolution. The ability to distinguish between these mechanistic classes underscores the importance of lipid composition in defining the local curvature landscape and the membrane's capacity to access different energetic pathways.

Our observations have led us to conclude the following:

1. Lipid membranes, even in the absence of proteins or imposed stresses, can act as active mechanical elements instead of being a passive scaffold for proteins to act upon and induce morphological complexities. Our findings align with growing evidence that lipid composition, curvature stress, and mechanical fluctuations can jointly drive shape selection and transformation.[5−7,12]
2. The observation of energetically neutral transformations leads us to conclude that these assemblies exist in energy landscapes with shallow minima, allowing small external perturbations to drive such transitions between quasi-stable configurations.
3. In vesicles containing lipids with mismatched phase behavior, transient mechanical perturbations may drive the assemblies up from a low-energy configuration, introducing geometric complexities. In this study, we have captured the relaxation of these assemblies from these higher energy levels, and this subsequent relaxation path, which we observed as a decline in total elastic energy tending toward an asymptote, appears to enable access to unexpected metastable morphologies, including toroidal shapes. These events were observed to occur in vesicles that did not show optically resolvable phase separation using phase-specific probes, consistent with the presence of solid-like domains below the optical resolution limit and slow lipid demixing kinetics as documented in prior literature.

These findings offer mechanistic insights into membrane shape evolution in both synthetic and biological systems and underscore the importance of curvature-composition coupling and mechanical stimuli in the context of lipid phase behavior, morphogenesis, and origins-of-life models.

ASSOCIATED CONTENT

Data Availability Statement

Excel document: Original quantitative imaging data for all assemblies.

Supporting Information

The Supporting Information is available free of charge at https://pubs.acs.org/doi/10.1021/acs.jpcb.5c05220.

Additional experimental details—Methods: vesicle preparation, confocal imaging; geometric analysis; energy calculations; trends in geometric and energetic parameters with time; supplementary Figures; geometric controls for axisymmetric analysis algorithm (PDF)

AUTHOR INFORMATION

Corresponding Authors

Akanksha Chauhan − *Kusuma School of Biological Sciences, Indian Institute of Technology Delhi, Delhi 110016, India;* orcid.org/0009-0006-2341-9260; Email: akanksha.chauhan@bioschool.iitd.ac.in

Aditya Mittal − *Kusuma School of Biological Sciences, Indian Institute of Technology Delhi, Delhi 110016, India;* orcid.org/0000-0002-4030-0951; Email: amittal@bioschool.iitd.ac.in

Complete contact information is available at: https://pubs.acs.org/10.1021/acs.jpcb.5c05220

Author Contributions

A.C. performed the standardization and production of GUVs along with the confocal imaging, algorithm design, code writing and data analyses. A.M. designed the study, provided resources, insights on data extraction, analyses, and conclusions. A.C. wrote the final version of the manuscript with inputs from A.M. Both the authors agreed on the final version of the manuscript.

Notes

The authors declare no competing financial interest.

ACKNOWLEDGMENTS

A.C. is grateful to Indian Institute of Technology Delhi for fellowship support and to Pragya for guidance on confocal imaging, and Professor V Haridas for access to the rotary evaporator. A.M. is grateful to Kusuma Trust (UK) for the financial support that enabled the establishment of the confocal microscopy facility. Authors are grateful to the Central Research

Facility and Kusuma School of Biological Sciences, IIT Delhi. A.M. dedicates this work to one of his closest friends, and a mentor (academic parent), Joseph E. Bentz (Joe) who passed away in late 2025 after seminally contributing to advancement of membrane biophysics (areas of membrane fusion and transport) for over 45 years. The authors are grateful to anonymous reviews that were very constructive and useful towards improving the overall readability of the manuscript.

■ ABBREVIATIONS

POPC, 1-palmitoyl-2-oleoyl-*sn*-glycero-3-phosphocholine; DOPE, 1,2-dioleoyl-*sn*-glycero-3-phosphoethanolamine; DPPC, 1,2-dipalmitoyl-*sn*-glycero-3-phosphocholine; Liss Rhod PE, 1,2-dioleoyl-*sn*-glycero-3-phosphoethanolamine-*N*-(lissamine rhodamine B sulfony)l; GUVs, giant unilamellar vesicles; L_o, ordered phase; L_d, disordered phase; Tm, melting temperature; *p*, perimeter; *a*, 2D enclosed area; *A*, 3D surface area; *V*, 3D volume; *E*, elastic energy; E_d, average elastic energy density

■ REFERENCES

(1) Deamer, D. The Role of Lipid Membranes in Life's Origin. *Life* **2017**, *7* (1), 5.
(2) Schrum, J. P.; Zhu, T. F.; Szostak, J. W. The Origins of Cellular Life. *Cold Spring Harbor Perspect. Biol.* **2010**, *2* (9), a002212.
(3) Canham, P. B. The Minimum Energy of Bending as a Possible Explanation of the Biconcave Shape of the Human Red Blood Cell. *J. Theor. Biol.* **1970**, *26* (1), 61−81.
(4) Helfrich, W. Elastic Properties of Lipid Bilayers: Theory and Possible Experiments. *Z. Naturforsch., C* **1973**, *28* (11−12), 693−703.
(5) Baumgart, T.; Hess, S. T.; Webb, W. W. Imaging Coexisting Fluid Domains in Biomembrane Models Coupling Curvature and Line Tension. *Nature* **2003**, *425* (6960), 821−824.
(6) Winter, A.; Liu, Y.; Ziepke, A.; Dadunashvili, G.; Frey, E. Phase Separation on Deformable Membranes: Interplay of Mechanical Coupling and Dynamic Surface Geometry. *Phys. Rev. E* **2025**, *111* (4), 044405.
(7) Yu, Q.; Košmrlj, A. Pattern Formation of Lipid Domains in Bilayer Membranes. *Soft Matter* **2025**, *21*, 4288.
(8) Hirst, L. S.; Ossowski, A.; Fraser, M.; Geng, J.; Selinger, J. V.; Selinger, R. L. B. Morphology Transition in Lipid Vesicles Due to In-Plane Order and Topological Defects. *Proc. Natl. Acad. Sci. U.S.A.* **2013**, *110* (9), 3242−3247.
(9) Lee, H. J.; Peterson, E. L.; Phillips, R.; Klug, W. S.; Wiggins, P. A. Membrane Shape as a Reporter for Applied Forces. *Proc. Natl. Acad. Sci. U.S.A.* **2008**, *105* (49), 19253−19257.
(10) Vlahovska, P. M. Asymmetric Shapes and Pearling of a Stretched Vesicle. *J. Fluid Mech.* **2014**, *754*, 1−4.
(11) Kudella, P. W.; Preißinger, K.; Morasch, M.; Dirscherl, C. F.; Braun, D.; Wixforth, A.; Westerhausen, C. Fission of Lipid-Vesicles by Membrane Phase Transitions in Thermal Convection. *Sci. Rep.* **2019**, *9*, 18808.
(12) Bansal, S.; Mittal, A. Extracting Curvature Preferences of Lipids Assembled in Flat Bilayers Shows Possible Kinetic Windows for Genesis of Bilayer Asymmetry and Domain Formation in Biological Membranes. *J. Membr. Biol.* **2013**, *246* (7), 557−570.
(13) Kubsch, B.; Robinson, T.; Steinkühler, J.; Dimova, R. Phase Behavior of Charged Vesicles Under Symmetric and Asymmetric Solution Conditions Monitored with Fluorescence Microscopy. *J. Vis. Exp.* **2017**, *128*, 56034.
(14) Bacellar, I. O. L.; Baptista, M. S. Mechanisms of Photosensitized Lipid Oxidation and Membrane Permeabilization. *ACS Omega* **2019**, *4* (26), 21636−21646.
(15) Parigoris, E.; Dunkelmann, D. L.; Murphy, A.; Wili, N.; Kaech, A.; Dumrese, C.; Jimenez-Rojo, N.; Silvan, U. Facile Generation of Giant Unilamellar Vesicles Using Polyacrylamide Gels. *Sci. Rep.* **2020**, *10* (1), 4824.
(16) Akashi, K.; Miyata, H.; Itoh, H.; Kinosita, K. Preparation of Giant Liposomes in Physiological Conditions and Their Characterization under an Optical Microscope. *Biophys. J.* **1996**, *71* (6), 3242−3250.
(17) Herold, C.; Chwastek, G.; Schwille, P.; Petrov, E. P. Efficient Electroformation of Supergiant Unilamellar Vesicles Containing Cationic Lipids on ITO-Coated Electrodes. *Langmuir* **2012**, *28* (13), 5518−5521.
(18) Zhou, Y.; Berry, C. K.; Storer, P. A.; Raphael, R. M. Peroxidation of Polyunsaturated Phosphatidyl-Choline Lipids during Electroformation. *Biomaterials* **2007**, *28* (6), 1298−1306.
(19) Breton, M.; Amirkavei, M.; Mir, L. M. Optimization of the Electroformation of Giant Unilamellar Vesicles (GUVs) with Unsaturated Phospholipids. *J. Membr. Biol.* **2015**, *248* (5), 827−835.
(20) Steinkühler, J.; De Tillieux, P.; Knorr, R. L.; Lipowsky, R.; Dimova, R. Charged Giant Unilamellar Vesicles Prepared by Electroformation Exhibit Nanotubes and Transbilayer Lipid Asymmetry. *Sci. Rep.* **2018**, *8* (1), 11838.
(21) Bagatolli, L. A.; Gratton, E. Two Photon Fluorescence Microscopy of Coexisting Lipid Domains in Giant Unilamellar Vesicles of Binary Phospholipid Mixtures. *Biophys. J.* **2000**, *78* (1), 290−305.
(22) Morales-Penningston, N. F.; Wu, J.; Farkas, E. R.; Goh, S. L.; Konyakhina, T. M.; Zheng, J. Y.; Webb, W. W.; Feigenson, G. W. GUV Preparation and Imaging: Minimizing Artifacts. *Biochim. Biophys. Acta Biomembr.* **2010**, *1798* (7), 1324−1332.
(23) Berndl, K.; Käs, J.; Lipowsky, R.; Sackmann, E.; Seifert, U. Shape Transformations of Giant Vesicles: Extreme Sensitivity to Bilayer Asymmetry. *Europhys. Lett.* **1990**, *13* (7), 659−664.
(24) Seifert, U. Vesicles of Toroidal Topology. *Phys. Rev. Lett.* **1991**, *66* (18), 2404−2407.
(25) McPhee, C. I.; Zoriniants, G.; Langbein, W.; Borri, P. Measuring the Lamellarity of Giant Lipid Vesicles with Differential Interference Contrast Microscopy. *Biophys. J.* **2013**, *105* (6), 1414−1420.
(26) Pazzi, J.; Subramaniam, A. B. Dynamics of Giant Vesicle Assembly from Thin Lipid Films. *J. Colloid Interface Sci.* **2024**, *661*, 1033−1045.
(27) Sankhagowit, S.; Wu, S.-H.; Biswas, R.; Riche, C. T.; Povinelli, M. L.; Malmstadt, N. The Dynamics of Giant Unilamellar Vesicle Oxidation Probed by Morphological Transitions. *Biochim. Biophys. Acta Biomembr.* **2014**, *1838* (10), 2615−2624.
(28) Tsuda, S.; Sakakura, T.; Fujii, S.; Suzuki, H.; Yomo, T. Shape Transformations of Lipid Vesicles by Insertion of Bulky-Head Lipids. *PLoS One* **2015**, *10*, No. e0132963.
(29) Coveas, J. L.; Milner, S. T.; Russel, W. B. Late Stages of the "Pearling" Instability in Lipid Bilayers. *J. Phys. II* **1997**, *7* (9), 1185−1204.
(30) Yanagisawa, M.; Imai, M.; Taniguchi, T. Shape Deformation of Ternary Vesicles Coupled with Phase Separation. *Phys. Rev. Lett.* **2008**, *100* (14), 148102.
(31) Fidorra, M.; Garcia, A.; Ipsen, J. H.; Härtel, S.; Bagatolli, L. A. Lipid Domains in Giant Unilamellar Vesicles and Their Correspondence with Equilibrium Thermodynamic Phases: A Quantitative Fluorescence Microscopy Imaging Approach. *Biochim. Biophys. Acta Biomembr.* **2009**, *1788* (10), 2142−2149.
(32) Svetlovics, J. A.; Wheaten, S. A.; Almeida, P. F. Phase Separation and Fluctuations in Mixtures of a Saturated and an Unsaturated Phospholipid. *Biophys. J.* **2012**, *102* (11), 2526.
(33) Wunderlich, B.; Leirer, C.; Idzko, A.-L.; Keyser, U. F.; Wixforth, A.; Myles, V. M.; Heimburg, T.; Schneider, M. F. Phase-State Dependent Current Fluctuations in Pure Lipid Membranes. *Biophys. J.* **2009**, *96* (11), 4592.
(34) Chernomordik, L. V.; Kozlov, M. M. Mechanics of Membrane Fusion. *Nat. Struct. Mol. Biol.* **2008**, *15* (7), 675−683.
(35) Vamparys, L.; Gautier, R.; Vanni, S.; Bennett, W. F. D.; Tieleman, D. P.; Antonny, B.; Etchebest, C.; Fuchs, P. F. J. Conical Lipids in Flat Bilayers Induce Packing Defects Similar to That Induced by Positive Curvature. *Biophys. J.* **2013**, *104* (3), 585−593.
(36) Pinot, M.; Vanni, S.; Ambroggio, E.; Guet, D.; Goud, B.; Manneville, J.-B. Feedback between Membrane Tension, Lipid Shape

https://doi.org/10.1021/acs.jpcb.5c05220
J. Phys. Chem. B 2025, 129, 12702−12714

and Curvature in the Formation of Packing Defects. *bioRxiv* **2018**, 389627.
(37) Hossein, A.; Beaven, A. H.; Sapp, K.; Sodt, A. J. Softening in Two-Component Lipid Mixtures by Spontaneous Curvature Variance. *J. Phys. Chem. B* **2024**, *128* (26), 6317−6326.
(38) Frolov, V. A. J.; Chizmadzhev, Y. A.; Cohen, F. S.; Zimmerberg, J. "Entropic Traps" in the Kinetics of Phase Separation in Multi-component Membranes Stabilize Nanodomains. *Biophys. J.* **2006**, *91* (1), 189−205.
(39) Elson, E. L.; Fried, E.; Dolbow, J. E.; Genin, G. M. Phase Separation in Biological Membranes: Integration of Theory and Experiment. *Annu. Rev. Biophys.* **2010**, *39*, 207−226.
(40) Bernchou, U.; Ipsen, J. H.; Simonsen, A. C. Growth of Solid Domains in Model Membranes: Quantitative Image Analysis Reveals a Strong Correlation between Domain Shape and Spatial Position. *J. Phys. Chem. B* **2009**, *113* (20), 7170−7177.
(41) Binder, W. H.; Barragan, V.; Menger, F. M. Domains and Rafts in Lipid Membranes. *Angew. Chem., Int. Ed. Engl.* **2003**, *42* (47), 5802−5827.
(42) Needham, D.; Nunn, R. S. Elastic Deformation and Failure of Lipid Bilayer Membranes Containing Cholesterol. *Biophys. J.* **1990**, *58* (4), 997−1009.
(43) Welti, R.; Glaser, M. Lipid Domains in Model and Biological Membranes. *Chem. Phys. Lipids* **1994**, *73* (1), 121−137.
(44) Mittal, A.; Chauhan, A. Aspects of Biological Replication and Evolution Independent of the Central Dogma: Insights from Protein-Free Vesicular Transformations and Protein-Mediated Membrane Remodeling. *J. Membr. Biol.* **2022**, *255* (2−3), 185−209.
(45) Bar-Ziv, R.; Moses, E. Instability and "Pearling" States Produced in Tubular Membranes by Competition of Curvature and Tension. *Phys. Rev. Lett.* **1994**, *73* (10), 1392−1395.
(46) Lentz, B. R.; Carpenter, T. J.; Alford, D. R. Spontaneous Fusion of Phosphatidylcholine Small Unilamellar Vesicles in the Fluid Phase. *Biochemistry* **1987**, *26* (17), 5389−5397.
(47) Noguchi, H.; Sakashita, A.; Imai, M. Shape Transformations of Toroidal Vesicles. *Soft Matter* **2015**, *11* (1), 193−201.
(48) Weakly, H. M. J.; Wilson, K. J.; Goetz, G. J.; Pruitt, E. L.; Li, A.; Xu, L.; Keller, S. L. Several Common Methods of Making Vesicles (except an Emulsion Method) Capture Intended Lipid Ratios. *Biophys. J.* **2024**, *123* (19), 3452−3462.
(49) Baumgart, T.; Hunt, G.; Farkas, E. R.; Webb, W. W.; Feigenson, G. W. Fluorescence Probe Partitioning between Lo/Ld Phases in Lipid Membranes. *Biochim. Biophys. Acta* **2007**, *1768* (9), 2182−2194.
(50) Sengupta, P.; Hammond, A.; Holowka, D.; Baird, B. Structural Determinants for Partitioning of Lipids and Proteins Between Coexisting Fluid Phases in Giant Plasma Membrane Vesicles. *Biochim. Biophys. Acta* **2008**, *1778* (1), 20−32.
(51) Subczynski, W. K.; Pasenkiewicz-Gierula, M.; Widomska, J.; Mainali, L.; Raguz, M. High Cholesterol/Low Cholesterol: Effects in Biological Membranes: A Review. *Cell Biochem. Biophys.* **2017**, *75* (3), 369−385.
(52) Boughter, C. T.; Monje-Galvan, V.; Im, W.; Klauda, J. B. Influence of Cholesterol on Phospholipid Bilayer Structure and Dynamics. *J. Phys. Chem. B* **2016**, *120* (45), 11761−11772.
(53) de Meyer, F.; Smit, B. Effect of Cholesterol on the Structure of a Phospholipid Bilayer. *Proc. Natl. Acad. Sci. U.S.A.* **2009**, *106* (10), 3654−3658.

https://doi.org/10.1021/acs.jpcb.5c05220
J. Phys. Chem. B 2025, 129, 12702−12714

Supporting information

Real-time confocal imaging of rare morphological transitions in protein-free GUVs uncovers shallow energy landscapes for membrane assemblies

Akanksha Chauhan**, Aditya Mittal*

Kusuma School of Biological Sciences, Indian Institute of Technology Delhi, New Delhi, 110016 India

* Correspondence: amittal@bioschool.iitd.ac.in

** Correspondence: akanksha.chauhan@bioschool.iitd.ac.in

Contents

A. Methods

i. Vesicle preparation:

The vesicle preparation was done by using the method described by Kubsch et al (2017).[8] The vesicles studied in this paper were of the composition: POPC: DPPC (9:1mol%), in 100 mM sucrose (+50mM KCl) aqueous system, at specific temperatures. These were labelled using LissRhodPE, (1/1000 w/w lipid content) that reliably segregates into the disordered liquid phase.

1. *Preparation of stocks*:
    i. 50 mM stocks of the lipids: POPC, DPPC (in methanol)
    ii. 1 mg/ml Liss- Rhod PE in methanol
2. *Lipid film deposition*:
    i. Took a round-bottom (RB) flask and covered it entirely (except the mouth) with an aluminum foil such that no light can enter.
    ii. Added 225 µL Chloroform + 15 µL Methanol to the RB flask.
    iii. Added 9 µL of POPC + 2 µL DPPC to the same flask.
    iv. 2 µL Liss- Rhod PE to the solution.
    v. Attached the RB to a rotary evaporator (roto-vap) set to 45°C and ran it for 4 minutes at 40 rpm under reduced pressure (100 mm Hg).
3. *Vacuum incubation*:

    Increased the temperature of the roto-vap to 60°C and incubated for 2 hours in reduced pressure state.
4. Sealed the tube under gaseous Nitrogen for transport between facilities.
5. *Pre- hydration:*
    i. Fit the RB in a glass beaker with deionized milli-Q water and unsealed the RB and sealed the beaker with 2 layers of cellophane sheets and tape.
    ii. Incubated the entire setup at 65 °C for 4 hours.
6. Prepared the aqueous phase during the pre-hydration incubation: 5 ml composed of 100 mM sucrose + 50 mM KCl
7. After the completion of the pre-hydration step, added 5 ml of aqueous phase slowly along the wall of the RB flask.
8. Sealed the flask quickly with a septum stopper and attached an argon (Ar) filled

balloon via a syringe.

9. Inserted another open-ended syringe to the stopper to allow the Ar to enter the flask.
10. Kept this setup at 65 ℃ for 5 mins.
11. Removed the open-ended syringe after 5 mins and kept the setup back in the incubator at 65 ℃ and incubated overnight (8-12 hours).
12. Removed the setup from the incubator and pipetted out the cloudy solution into glass vials.
13. Observed the preparations under a confocal microscope with 543nm laser and with Differential interference contrast (DIC).

ii. Confocal Imaging:

The prepared vesicles were imaged via confocal microscopy- using Olympus FV1200 (543nm; Evolve Delta, Photometrics®) and the softwares- Fluoview 4.1.2.2 and Olympus cellSens Dimension 1.9 (© 2009-2013). DIC images of the same were captured simultaneously while epifluorescence imaging was done separately.

Table S1: Imaging specifications

	Event A	Event B	Event C	Event D	Event E
Time parameter	3.38 s/ Frame	3.38 s/ Frame	1.15 s/ Frame	3.38 s/ Frame	1.7 s/ Frame
Bits/Pixel	12 [bits]	12 [bits]	12 [bits]	12 [bits]	12 [bits]
Size (pixels)	512 x 512 [Pixel] 0.248 [µm/Pixel]	512 x 512 [Pixel] 0.248 [µm/Pixel]	512 x 512 [Pixel] 0.062 [µm/Pixel]	512 x 512 [Pixel] 0.082 [µm/Pixel]	512 x 512 [Pixel] 0.08 [µm/Pixel]
Objective lens	ULSAPO100x O (N.A.- 1.40)	ULSAPO100x O (N.A.- 1.40)	ULSAPO100x O (N.A.- 1.40)	ULSAPO100x O (N.A.- 1.40)	ULSAPO100x O (N.A.- 1.40)
Channel1	Excitation: 543 nm Emission: 578 nm	Excitation: 543 nm Emission: 578 nm	Excitation: 543 nm Emission: 578 nm	Excitation: 543 nm Emission: 578 nm	Excitation: 543 nm Emission: 578 nm
TD1 channel	DIC	DIC	DIC	DIC	DIC
Sampling speed	4.0 [µs/Pixel]	4.0 [µs/Pixel]	2.0 [µs/Pixel]	4.0 [µs/Pixel]	2.0 [µs/Pixel]

Temperature	25 ℃	25 ℃	25 ℃	25 ℃	25 ℃

iii. Geometric analysis:

Axisymmetric assemblies: The membrane was traced and the field was cropped using a semi-automated MATLAB algorithm to generate clean images for further processing.

2D analysis:

Once the object was segmented and the region of interest identified using thresholding. The perimeter, area and circularity were calculated using the regionprops function in MATLAB.

3D:

Surface area– The boundary points of the object were determined, and the object was moved to place the centroid at [0,0] and have the major axis align with the y axis. The absolute values of the resultant x and y coordinates of the boundary points were saved in separate arrays. dx and dy were calculated and subsequently the hypotenuse was calculated as $dl = \sqrt{dx^2 + dy^2}$. Radial distance of dl from the axis of symmetry was calculated as $r = x + \frac{dx}{2}$. The area of the ring formed by rotation of this section is calculated by $ds = \pi * dx * dl$, and the sum of ds across the boundary gives the surface area. The surface area was scaled from pixels to µm units.

Volume– Volume of the ring formed by rotation of this section is calculated by $dv = \frac{\pi}{2} * dx^2 * dl$, and the sum of dv across the boundary gives the total volume of the rotated 3D object. The volume was scaled from pixels to µm units.

Non-axisymmetric assemblies

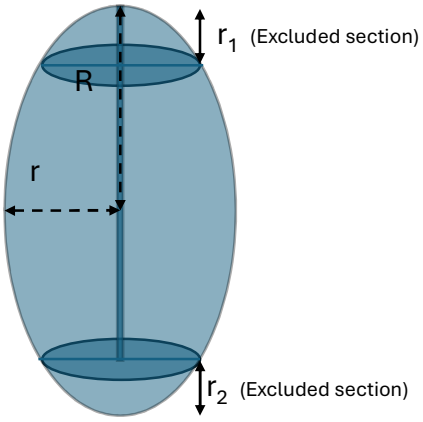

Figure S1 Ellipsoidal sections

Ellipsoidal sections

R, r, r1 and r2 of the ellipsoidal sections are measured manually for each section. Distance of the excluded sections from the center are calculated as h1= R- r1 and h2= R- r2. e is calculated as:

$$e = \sqrt{1 - \frac{r^2}{R^2}}$$

2D perimeter– $p = 2\pi * \sqrt{\frac{R^2+r^2}{2}}$

2D area– $a = \frac{r}{R}\int_{-h_2}^{h_1} \sqrt{R^2 - x^2}\, dx$

3D Surface area– $A = 2\pi\frac{r}{R}\int_{-h_2}^{h_1} \sqrt{R^2 - x^2 * \frac{(R^2-r^2)}{R^2}}\, dx$

3D Volume– $V = \pi\frac{r^2}{3R^2}(3R^2(h_1 + h_2) - {h_2}^2 - {h_1}^2)$

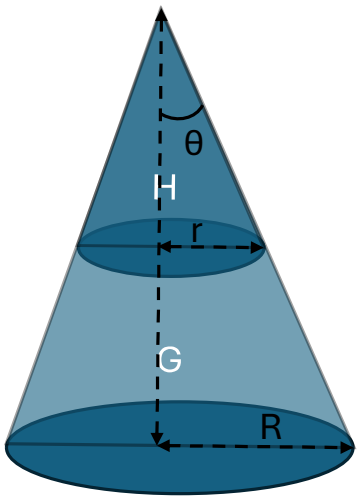

Figure S2 Conic sections

Conic sections

The R, r and H (height of the bigger cone) were measured manually.

2D perimeter– $p = 2(R^2 - r^2)\sin\theta$

2D area– $a = \frac{H}{2R}(R^2 - r^2)$

3D Surface area– $A = \pi\frac{(R^2-r^2)}{\sin\theta}$

3D Volume– $V = \pi\frac{(R^3-r^3)}{3\sin\theta}$

Tubular sections:

The height (H) and the Radius (R) were manually calculated.

2D perimeter– $p = 2\mathrm{H}$

2D area– $a = 2R\mathrm{H}$

3D Surface area– $A = 2\pi R\mathrm{H}$

3D Volume– $V = \pi R^2 H$

Toroidal :

Radius of the inner circle (r') and outer circle (R') were manually measured. The radius of the toroidal tube (r) is calculated as :

$$r = \frac{R'-r'}{2}$$

The distance from the centroid to the middle of the tube (R) is calculated as:

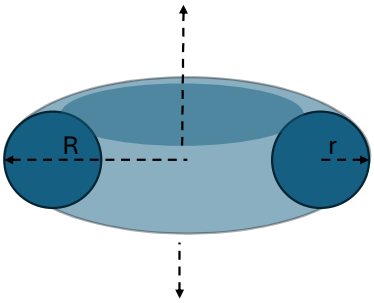

$R = R' - r$

2D perimeter– $p = 2\pi(R' + r')$

2D area– $a = \pi(R'^2 - r'^2)$

3D Surface area– $A = 4\pi^2 R\mathrm{r}$

3D Volume– $V = 2\pi^2 R r^2$

Figure S3 Toroidal sections

iv. Energy calculations

Axisymmetric assemblies

The boundary points retrieved for the geometric parameters were used, after scaling to μm. The boundary was divided into two halves to take into account any differences in two halves of the membrane boundaries. The boundary points positive half, after moving the object to have the centroid at the [0,0], is isolated. These points are then rotated around the major axis, and the z-coordinates are obtained, and the 3D coordinates are calculated accordingly. These coordinates are compiled to give the vertices and the faces are calculated using the convex hull function (convhull). The triangulation of these vertices and faces is created using the inbuilt triangulation function of MATLAB and the face areas are calculated for the whole . The 'patchcurvature' function is used to calculate the mean curvature and gaussian curvature at each point. The bending constant (κ) value used were 21 kBT for POPC:DOPE and 28.6 kBT for POPC:DPPC and the Co was assumed to be 0 since the membranes were symmetric. The energy density is then calculated as $dE = \frac{\kappa}{2}(2C_m - C_0)^2$, which is then integrated across the triangulation to give the total elastic energy of the first half (positive half). Similarly, the elastic energy of the second half (negative half) is calculated, and the average of the two halves is calculated to give the final elastic energy of the whole assembly.

Non-axisymmetric assemblies

The elastic energy of the individual sections are calculated and then added up to give the total elastic energy of the assembly.

Ellipsoidal sections

$$E = \frac{\kappa}{2}\left(\frac{1}{R}+\frac{1}{r}\right)^2 A$$

Conic sections

$$E = 2\pi\kappa\left(\frac{\log(R)-\mathrm{l}\quad(r)}{\mathrm{si}}\right)$$

Tubular sections

$$E = \frac{\kappa}{2}\left(\frac{1}{R}\right)^2 A$$

Torus

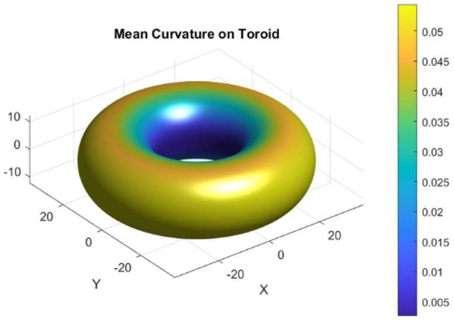

Figure S4 Mean curvature calculated for torus

$$E = 2\pi rk\left[\left(\int_{(R-r)}^{R}\frac{x}{\sqrt{r^2-(x-R)^2}}\left(\frac{1}{r}-\frac{1}{(x)}\right)^2 \mathrm{d}x\right)\right.$$
$$\left.+\left(\int_{R}^{(R+r)}\frac{x}{\sqrt{r^2-(x-R)^2}}\left(\frac{1}{r}+\frac{1}{(x)}\right)^2 \mathrm{d}x\right)\right]$$

B. Trends in geometric and energetic parameters with time

The complete raw quantitative data (geometric and energetic) can be found in the supplementary excel sheet.

Event-A

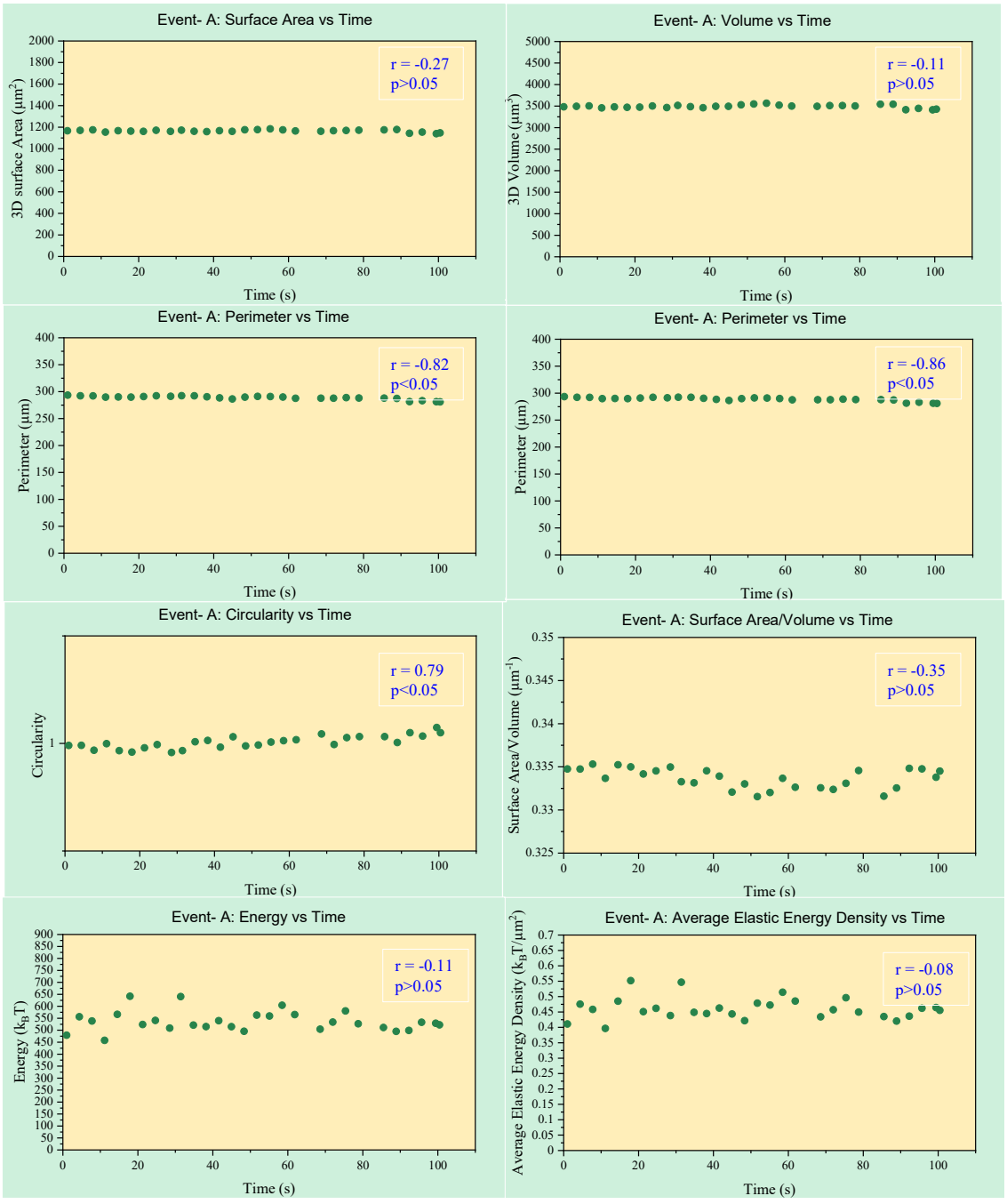

Figure S5 Event A energetic and geometric parameter changes with time

Event B

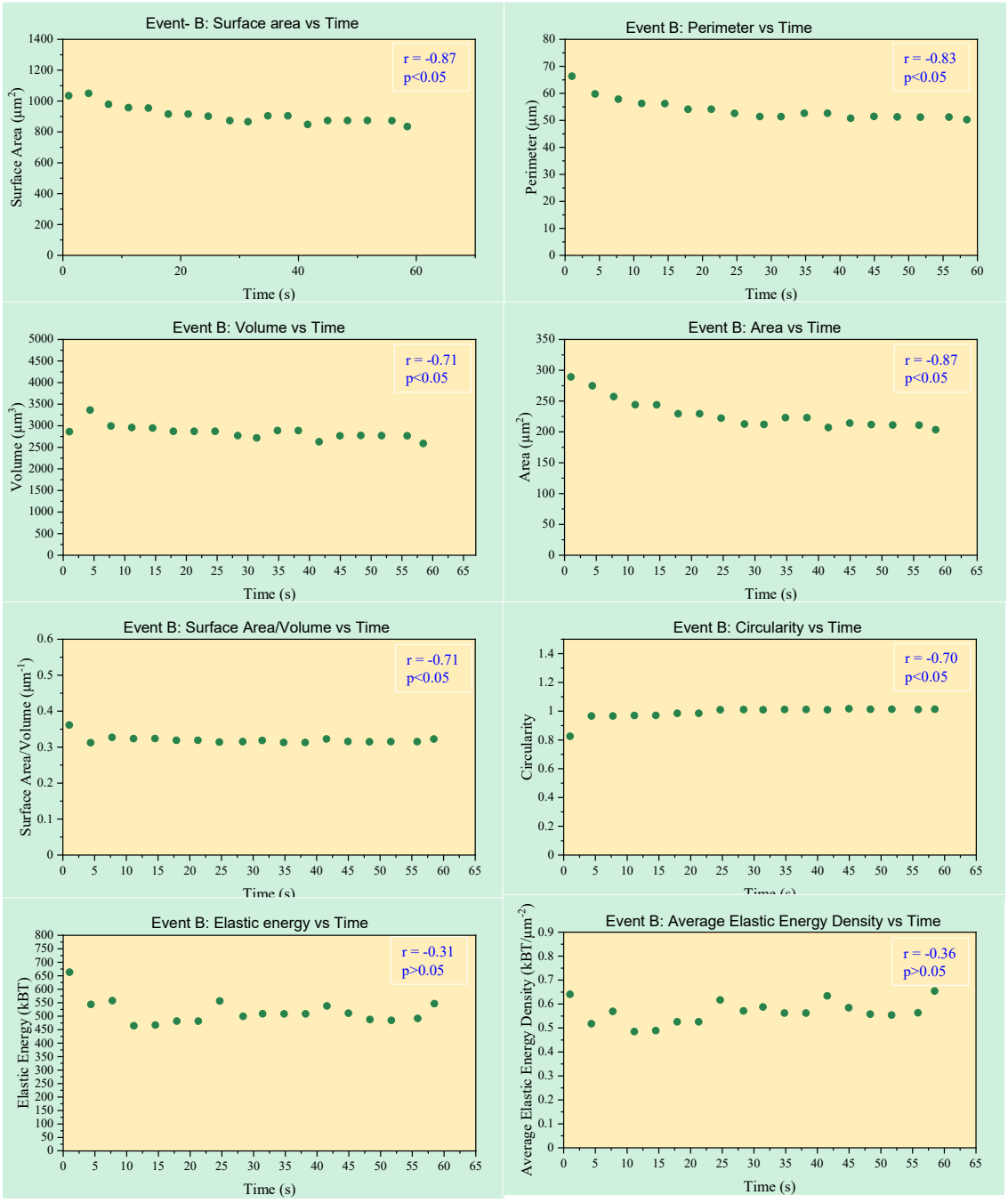

Figure S6 Event B energetic and geometric parameter changes with time

Event C

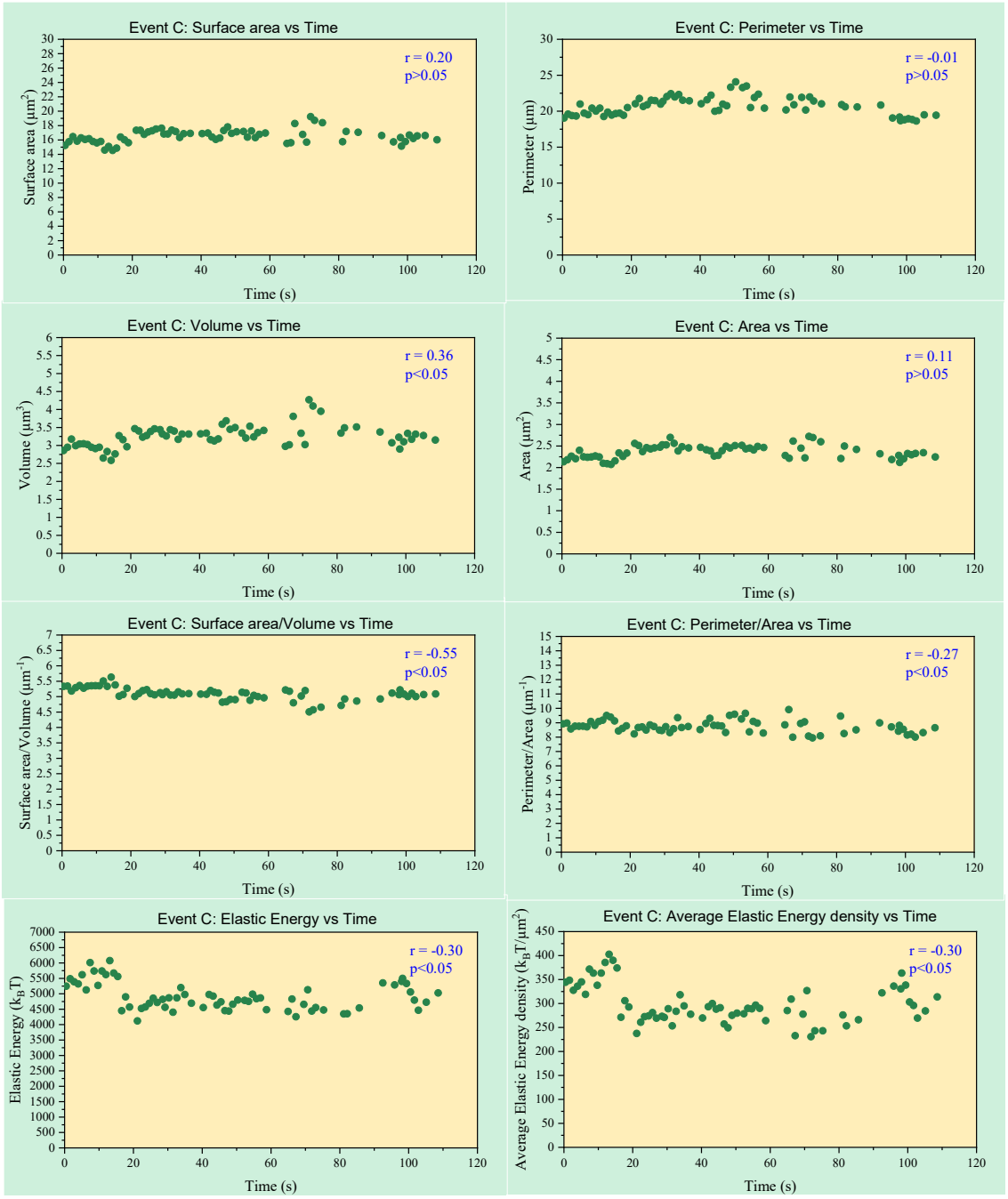

Figure S7 Event C energetic and geometric parameter changes with time

Event D

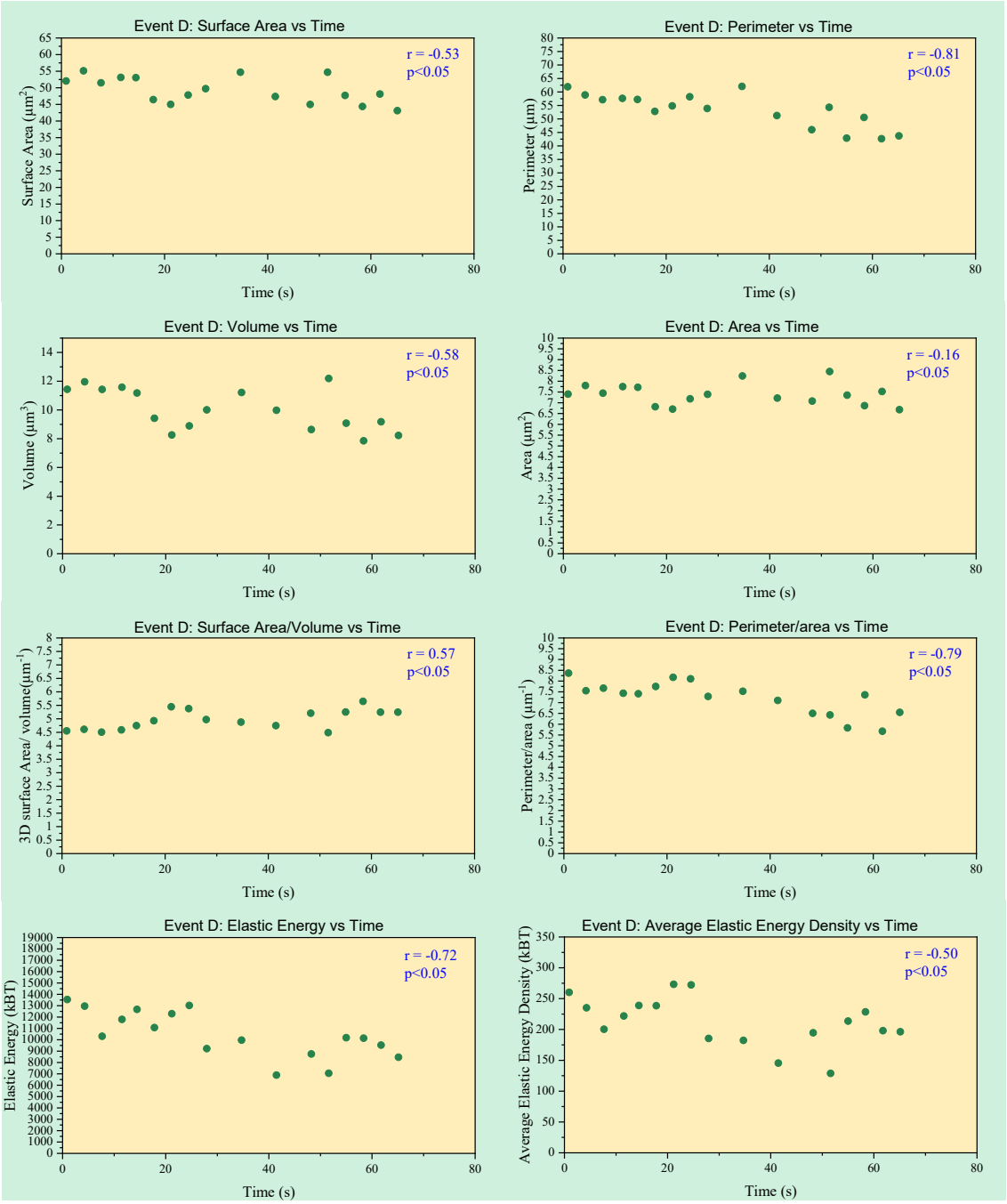

Figure S8 Event D energetic and geometric parameter changes with time

Event E

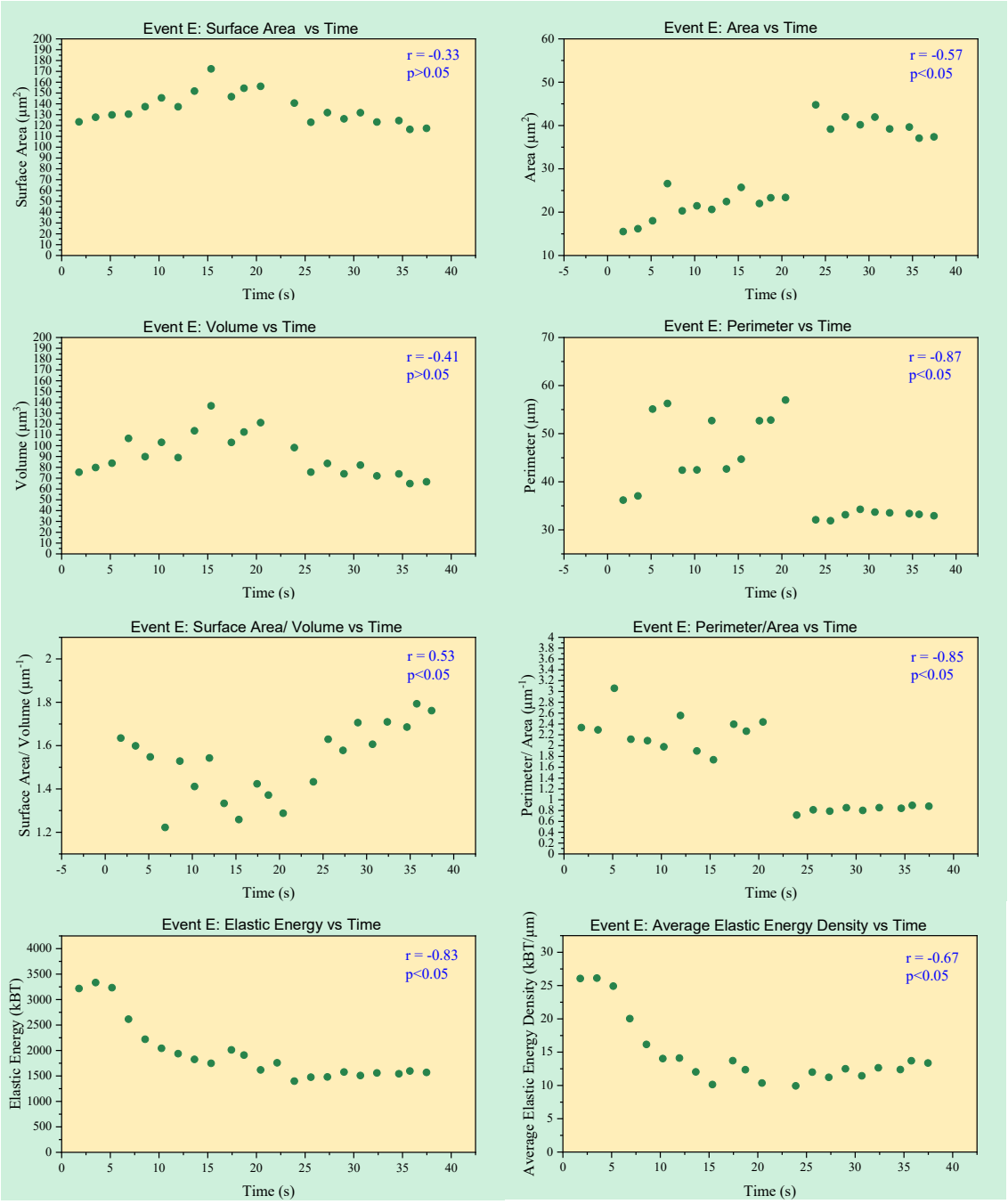

Figure S9 Event E energetic and geometric parameter changes with time

C. Supplementary Figures

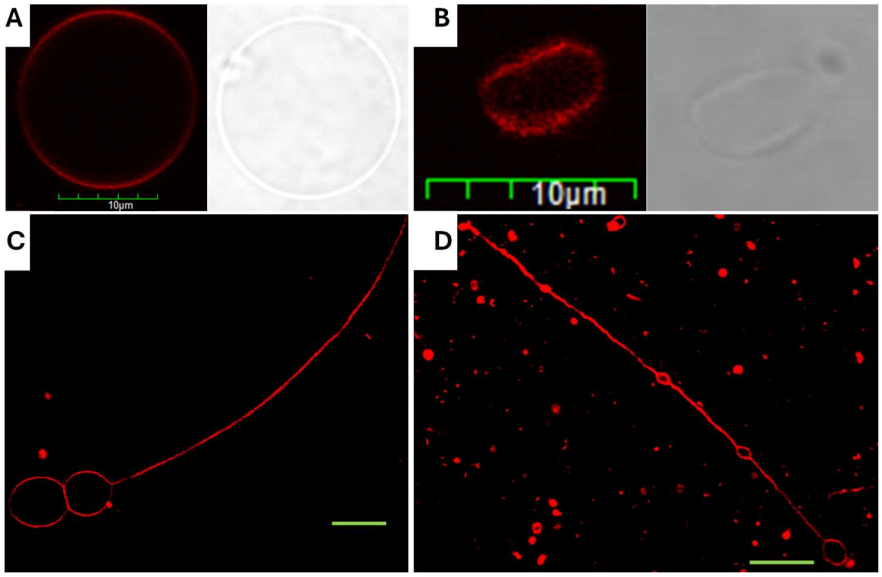

Figure S10 Confocal microscopy images of assemblies without expected phase separation (POPC: DOPE (9:1)) observed: A- spherical, B- oblong, C- Tube, D- pearling. Green bar= 10 µm

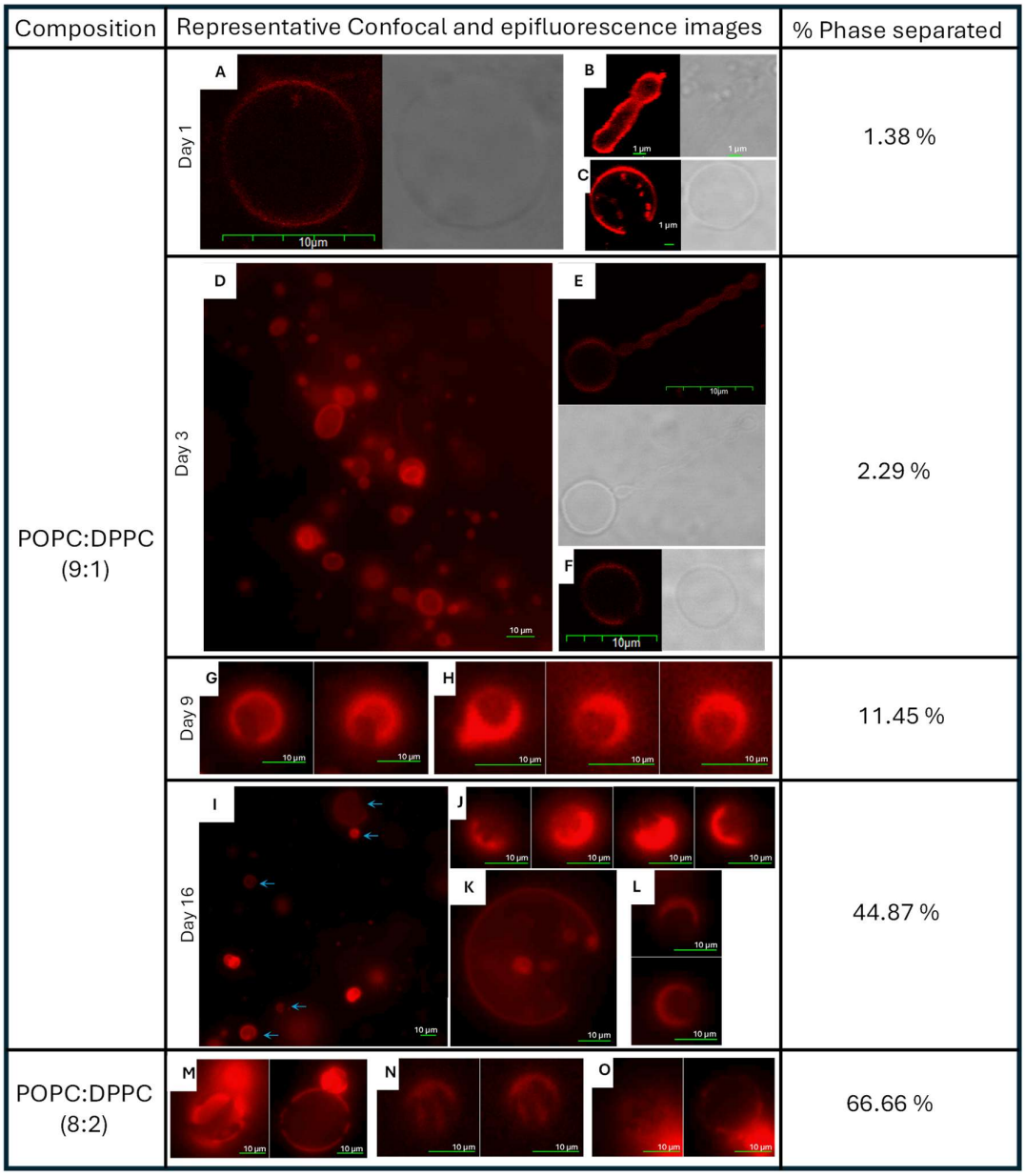

Figure S11 POPC: DPPC vesicles (liquid disordered: solid ordered phase separating GUVs) observed at different time points, with respective fractions of phase separated assemblies in the third column. (A-L) have (9:1) ratio of POPC:DPPC and (M-O) have (8:1) ratio. (9:1)- Day 1 (A, B) assemblies exhibited spherical (A), oblong (B) and phase separated (C) vesicles in addition to pearling (event-C, D). Day 3 (D-F) assemblies exhibited oblong & spherical(D), pearling (E), phase separated (F) vesicles. Day 9 (G,H) exhibited increased number of phase-separated vesicles, with solid phase exhibiting bar-like (G) and triangular (H) shapes in addition to spherical vesicles with no phase separation and vesicles with circular solid phases. Day 27 (I-L) exhibited an even higher frequency of vesicles exhibiting solid phases (I). Solid phase was observed in snowflake-like(J) shape in addition to circular (L) shape. The curvature close to the phase boundary in bigger vesicles was observed to be greater in Ld phase (C, K, M and O) in accordance with the line-tension theory by Baumgart et al (2003)[5]. A lower yield

of (8:2) assemblies was observed with majority of vesicles exhibiting solid phase in striped or webbed shapes (M-O) in agreement with concentration dependent pattern formation observed in liquid-liquid phase separation.

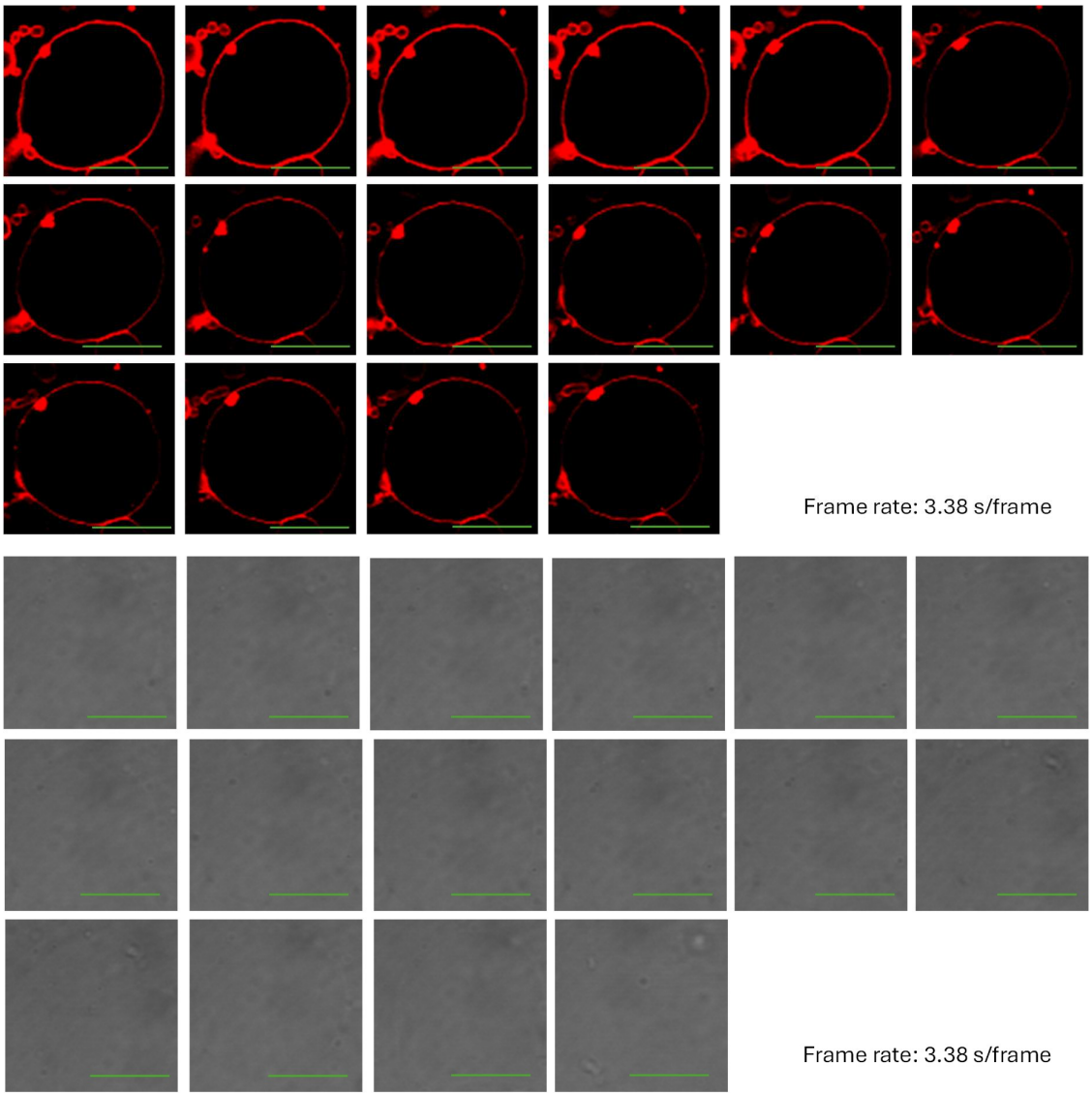

Figure S12: All frames of event A: Confocal and DIC (green bar= 10 μm); frame rate=3.38 s/frame

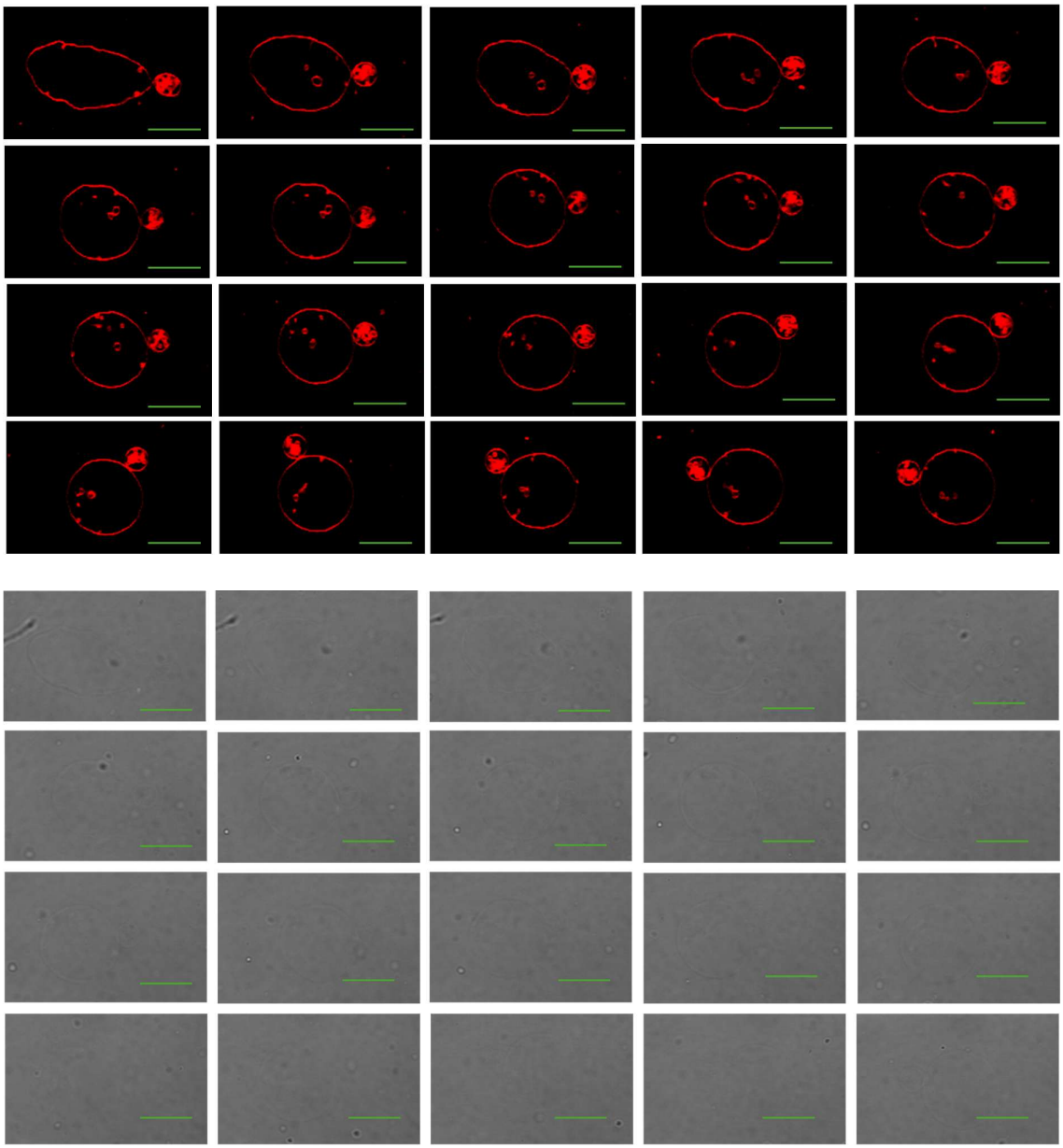

Figure S13: All frames of event B: Confocal and DIC (green bar= 10 µm); frame rate=3.38 s/frame

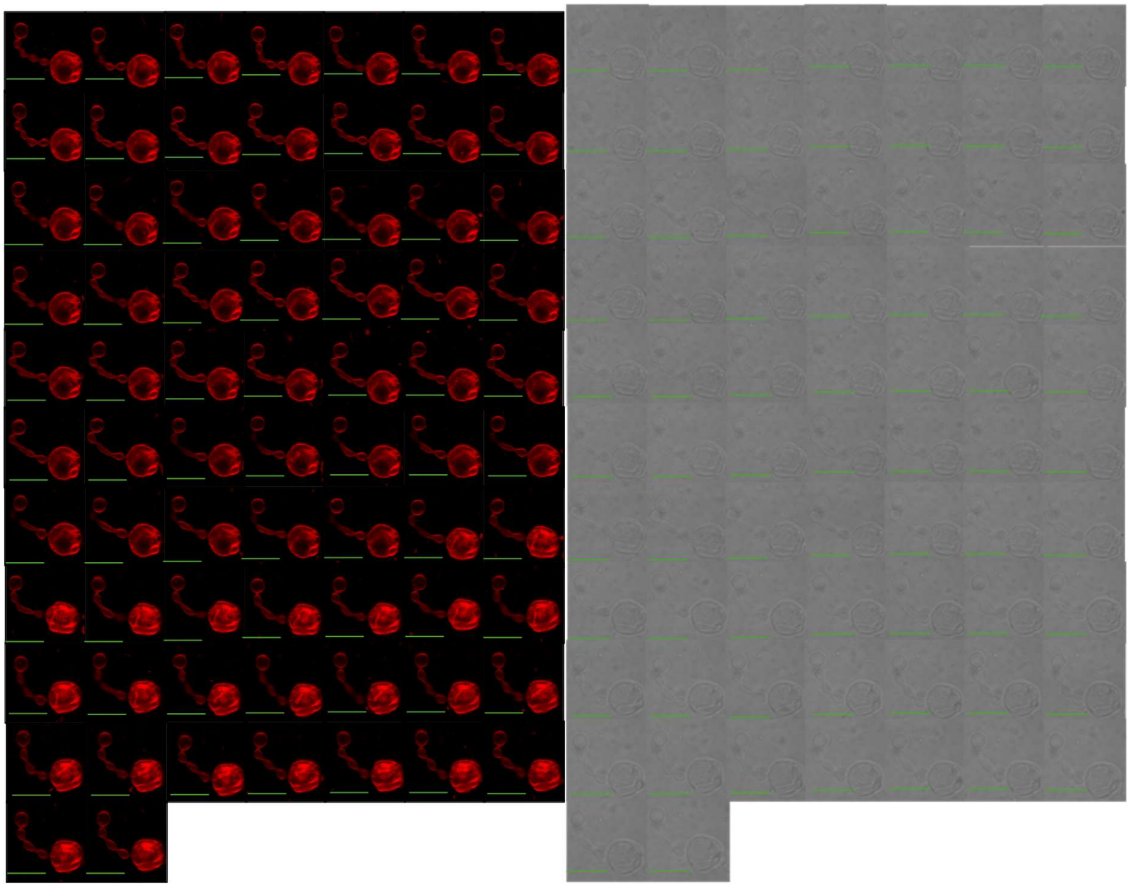

Figure S14: All frames of event C: Confocal and DIC (green bar= 5 µm) ; frame rate=1.15 s/frame

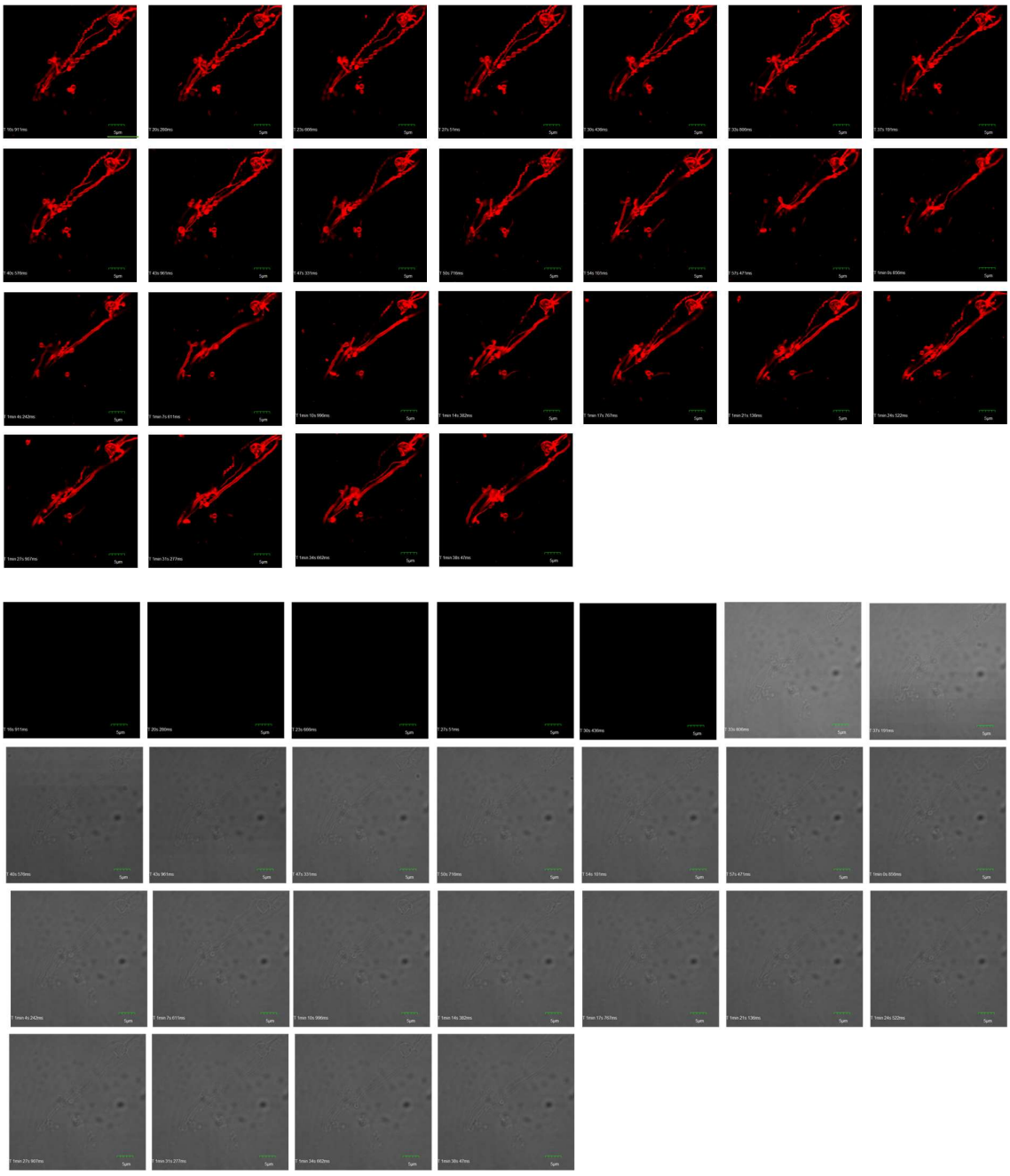

Figure S15: All frames of event D: Confocal and DIC (green bar= 5 µm). frame rate=3.38 s/frame

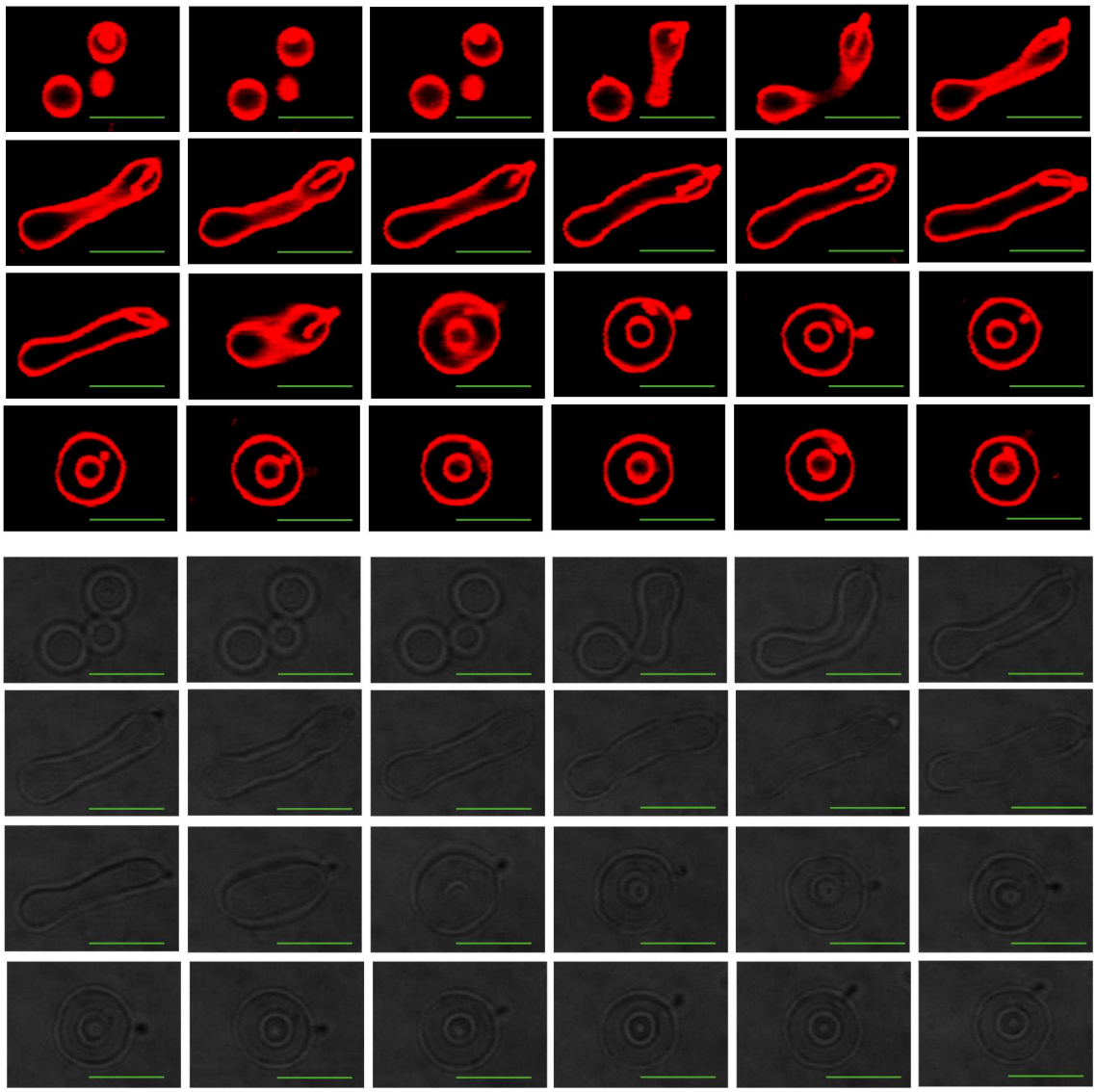

Figure S16: All frames of event E: Confocal and DIC (green bar= 10 μm) frame rate=1.7 s/frame

D. Geometric controls for axisymmetric analysis algorithm

2D controls

2D shapes were generated while keeping the perimeter constant, and the number of vertices were increased from 3 to 50. The area and perimeter values were recorded using the automated algorithm for axisymmetric vesicles.

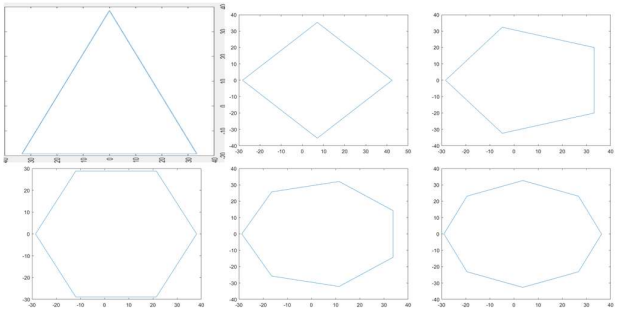

Figure S17 2D shapes generated as computational controls

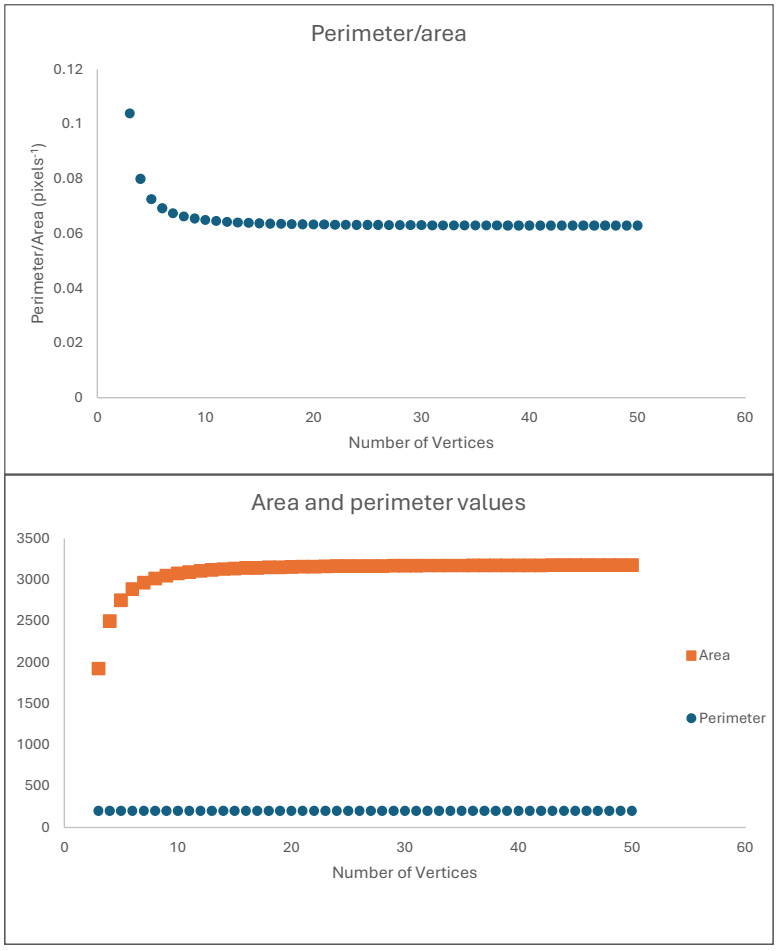

Figure S18 2D parameter graphs for controls with increasing number of vertices

3D controls

The shapes were rotated around their major axis to give a projection. The volume and surface area of these projections were calculated using the same algorithm that was used to create projections and calculate 3D surface area and volume values of the imaging data.

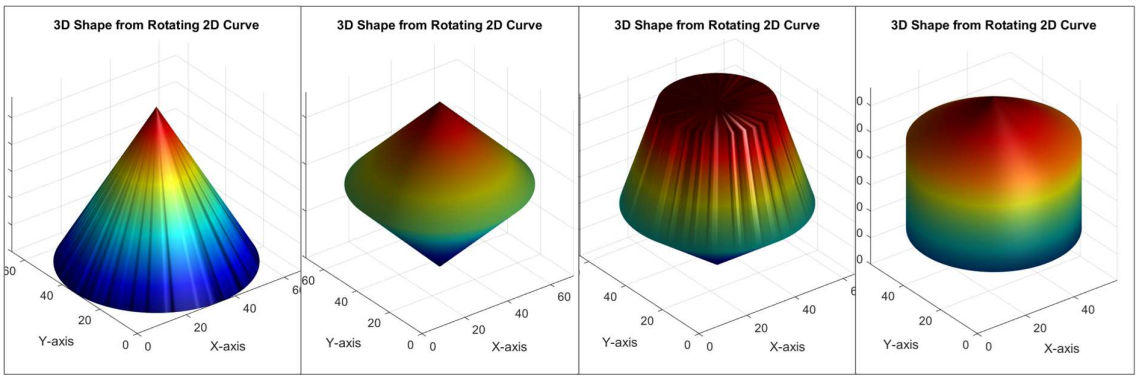

Figure S19 3D shaped generated as computational controls

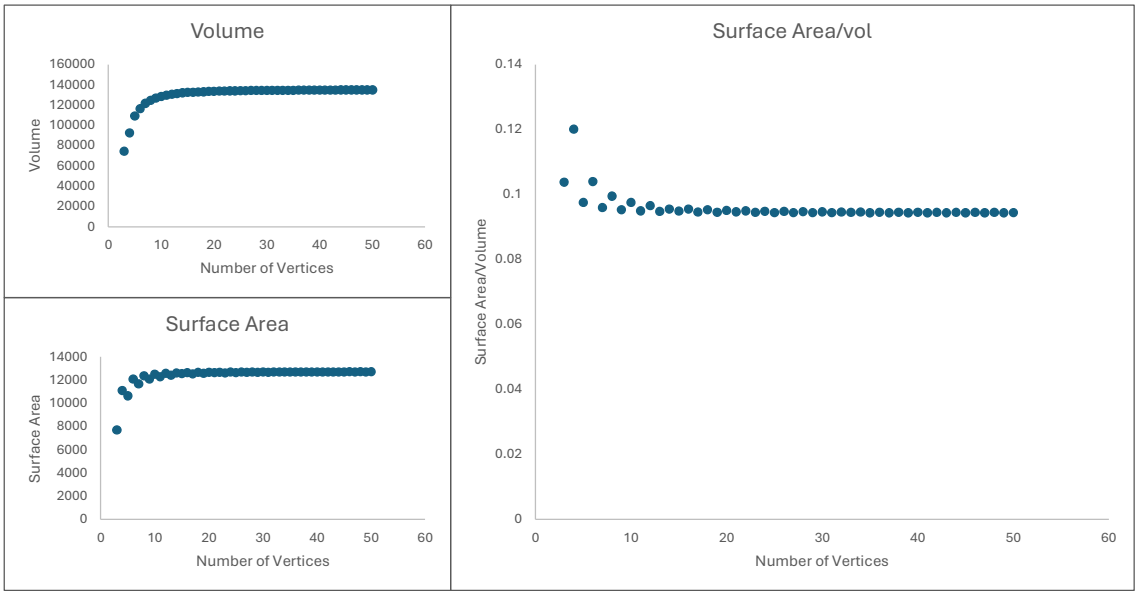

Figure S20 3D geometric parameter graphs for controls with increasing number of vertices